frontiers | Frontiers in Environmental Science

TYPE Original Research
PUBLISHED 10 March 2025
DOI 10.3389/fenvs.2025.1547530

OPEN ACCESS

EDITED BY
Xiuping Li,
Chinese Academy of Sciences (CAS), China

REVIEWED BY
Muhammad Shahid,
Brunel University London, United Kingdom
Subhanil Guha,
National Institute of Technology Raipur, India

*CORRESPONDENCE
Zhang Lu,
syxyzxy@163.com

RECEIVED 19 December 2024
ACCEPTED 06 February 2025
PUBLISHED 10 March 2025

CITATION
Lu Z (2025) Application of remote sensing technology in studying the interaction between culture and environment in the Third Pole Region.
Front. Environ. Sci. 13:1547530.
doi: 10.3389/fenvs.2025.1547530

Application of remote sensing technology in studying the interaction between culture and environment in the Third Pole Region

Zhang Lu*

Jiangmen Polytechnic, Jiangmen, Guangdong, China

Introduction: The interplay between cutture and environment in the Third Pole Region holds profound implications for the region's socio-ecological resilience and long-term sustainability. However, existing research has largely relied onisolated analyses, often constrained by the absence of integrative frameworks capable of capturing the dynamic and interdependent nature of cultural and environmental systems. These conventional approaches frequently overlook the spatial-temporal complexity, synergistic relationships, and feedback mechanisms intrinsic to this interplay, thereby limiting their predictive accuracy and adaptability in addressing emerging challenges.

Methods: To bridge these gaps, we propose the Dynamic Cultural-Environmental Interaction Network (DCEN), a novel computational framework that integrates cultural metrics and environmental variables within a graph-based, multidimensional model. This approach systematically captures bidirectional interactions through coupled nonlinear equations, incorporating spatial and temporal dynamics while accounting for external stimuli and abrupt perturbations. Furthermore, we introduce the Adaptive Interaction Strategy for Cuttural-Environmental Systems (AIS-CES), which enables real-tme optimization of model parameters based on system feedback, ensuring stability, adaptability, and enhanced resilience.

Results: Experimental validation demonstrates that the proposed framework effectively simulates complex cultural-environmental interactions with high predictive accuracy, providing a robust foundation for policymaking, adaptive management, and disaster mitigation in the Third Pole Region.

Discussion: By addressing critical limitations in existng methodologies, this research advances a more holistic and actionable understanding of cultural-environmental dynamics, fostering regional sustainability and socio-ecological harmony.

KEYWORDS

culture-environment interactions, dynamic networks, Third Pole Region, computational modeling, adaptive strategies

1 Introduction

The Third Pole region, encompassing the Himalayas and surrounding areas, plays a critical role in global climate regulation, ecological balance, and cultural diversity (Isensee et al., 2020). Its unique topography and climatic conditions not only influence local ecosystems but also sustain ancient cultural traditions deeply intertwined with the environment (Cao et al., 2021). Studying the interaction between culture and the environment in this region is vital for understanding how climate change, urbanization, and socio-economic shifts impact these delicate balances (Minaee et al., 2020). Traditional field-based studies are not only labor-intensive but also often restricted by the remoteness and harshness of the region (Cheng et al., 2021). Remote sensing technology offers a transformative solution by enabling large-scale, continuous monitoring of environmental and cultural patterns (Hatamizadeh et al., 2021). It not only facilitates the collection of high-resolution spatial and temporal data but also supports the integration of diverse datasets, offering deeper insights into the dynamic interactions between human societies and their environment in this fragile region.

To address the limitations of earlier methods, researchers initially relied on traditional symbolic AI and knowledge-based systems to study cultural and environmental interactions (Xu et al., 2023). These approaches focused on creating rule-based models that incorporated expert knowledge to analyze cultural and ecological phenomena (Huang et al., 2020). For example, early systems used symbolic representations to map historical land-use patterns or trace changes in sacred landscapes (Valanarasu and Patel, 2022). While these methods offered interpretable insights and highlighted the role of specific cultural practices in shaping the environment, they were constrained by their reliance on predefined rules and static datasets (Yu et al., 2023). The lack of scalability and adaptability to emerging complexities limited their effectiveness in capturing the dynamic and multi-dimensional nature of the Third Pole's cultural-environmental interactions (Valanarasu et al., 2021).

The advent of data-driven approaches and machine learning marked a significant shift in remote sensing applications for this research area (Zhang Y. et al., 2021). Data-driven methods leveraged large-scale geospatial datasets to uncover patterns and correlations without explicit rule-based programming (Xie et al., 2021). Machine learning algorithms enabled automated classification of land use, detection of environmental changes, and identification of anthropogenic impacts on cultural sites (Wang et al., 2021). For instance, support vector machines and random forests were commonly employed to analyze satellite imagery, allowing researchers to detect subtle cultural markers such as terraced farming or sacred groves (Ghiasi et al., 2021). Despite these advancements, the dependency on labeled datasets and the difficulty of interpreting machine learning models posed challenges (Jain et al., 2022). Furthermore, these approaches often struggled to incorporate the rich contextual and temporal nuances necessary for understanding the interplay between culture and the environment.

The emergence of deep learning and pre-trained models revolutionized the field by offering unparalleled capabilities in feature extraction and pattern recognition (Müller et al., 2022). Neural networks, particularly convolutional neural networks (CNNs), excelled at processing high-resolution remote sensing imagery to identify intricate cultural and environmental features (Yin et al., 2022). Pre-trained models, such as those based on transfer learning, facilitated the integration of multispectral and temporal data, enabling robust analysis of complex phenomena like cultural heritage conservation amidst climate change (Wu et al., 2022). These methods also supported the development of multi-modal frameworks that combined remote sensing with ethnographic and historical data (Zhang W. et al., 2021). However, deep learning models often suffered from high computational costs and limited interpretability, necessitating efforts to balance accuracy with transparency (Malhotra et al., 2022). The lack of generalized datasets tailored to the Third Pole's unique characteristics also highlighted the need for more customized solutions.

Based on the aforementioned limitations, this study proposes a novel framework that integrates the strengths of deep learning with domain-specific cultural and environmental knowledge to overcome existing gaps. Our approach combines pre-trained neural networks with tailored data augmentation techniques to capture the diverse and dynamic nature of the Third Pole region. by incorporating hybrid models that merge statistical and rule-based systems, we address the challenges of interpretability and context-awareness. This method not only enhances the scalability of remote sensing applications but also ensures that cultural insights are preserved in the analysis.

- The proposed method integrates domain-specific knowledge with advanced deep learning, offering a unique approach to analyzing culture-environment interactions.
- The framework is designed for efficient and versatile application across diverse datasets and scales, making it suitable for various cultural and environmental contexts.
- Preliminary results demonstrate superior accuracy and reliability in detecting and interpreting complex patterns in the Third Pole region compared to traditional methods.

2 Related work

2.1 Remote sensing for cultural landscape analysis

Remote sensing technologies have increasingly been utilized to analyze cultural landscapes, enabling the study of human-environment interactions at a regional scale (Jha et al., 2020). In the Third Pole region, cultural landscapes are heavily influenced by environmental conditions, traditional practices, and socio-economic dynamics (Luo et al., 2020). By employing high-resolution satellite imagery and geospatial analysis, researchers can identify patterns of settlement distribution, agricultural practices, and infrastructure development that reflect the adaptation of human populations to the unique environmental conditions of this area (Lüddecke and Ecker, 2021). For example, spectral indices such as the Normalized Difference Vegetation Index (NDVI) allow for the mapping of cultivated lands and pasturelands, providing insights into traditional subsistence strategies (Wang et al., 2024). The integration of temporal remote sensing data further supports the monitoring of changes in cultural landscapes over time, such as shifts in land use driven by climate change, policy interventions, or economic development (Wang et al., 2023). Beyond physical mapping, remote sensing supports the identification of intangible cultural features by assessing proxies such as the spatial arrangement of religious sites, traditional architecture, and sacred natural sites. Multispectral and hyperspectral imaging techniques reveal the material composition of historical and cultural structures,

enabling conservation and heritage management. Combined with ground-truthing and ethnographic studies, remote sensing data contribute to a holistic understanding of how cultural landscapes are shaped and maintained in response to environmental dynamics. As the Third Pole faces increasing pressures from climate change and modernization, remote sensing provides a crucial tool for documenting and preserving the cultural heritage embedded in its landscapes.

2.2 Environmental change and cultural adaptation

Remote sensing is a powerful tool for studying environmental changes and their impact on cultural systems, especially in the Third Pole region, where rapid environmental transformations are occurring (Chaitanya et al., 2020). Glacier retreat, permafrost thaw, and alterations in hydrological systems are key environmental changes that significantly affect human livelihoods and cultural practices (Atigh et al., 2022). Satellite-based remote sensing, including data from Landsat, Sentinel, and MODIS platforms, enables the detection and quantification of these changes with high temporal and spatial resolution (Chen et al., 2020). For instance, glacier monitoring using Synthetic Aperture Radar (SAR) and optical imagery has revealed significant ice loss in the Himalayas, directly impacting water availability for downstream communities (Wang et al., 2022). The implications of such environmental changes on cultural adaptation can be examined through remote sensing by linking ecological variables with human activities (Jiang et al., 2024). For example, remote sensing of vegetation cover can illustrate the resilience or vulnerability of traditional pastoral systems to climatic stressors. Changes in river dynamics, detectable through remote sensing, reveal the effects on irrigation-dependent agricultural practices that are central to local cultures. Remote sensing also supports the study of disaster impacts on cultural systems, such as landslides or floods, providing data critical for understanding recovery processes and long-term adaptations. By integrating remote sensing with socio-cultural data, researchers gain insights into how communities in the Third Pole adapt their cultural practices in response to environmental challenges.

2.3 Sacred natural sites and environmental monitoring

Sacred natural sites, often associated with religious and cultural significance, serve as critical nodes of cultural-environmental interaction in the Third Pole region (Ouyang et al., 2020). Remote sensing technologies provide an effective means to study these sites, their environmental settings, and the surrounding landscapes (Gao et al., 2021). High-resolution imagery and LiDAR data are particularly useful for delineating sacred sites and analyzing their spatial relationships with ecological features such as water bodies, forests, and mountain peaks (Lin et al., 2021). These analyses reveal how sacred natural sites are integrated into broader cultural and ecological systems, reflecting traditional beliefs about the environment (Liu et al., 2021). Remote sensing also facilitates the monitoring of environmental conditions around sacred natural sites, supporting conservation efforts and understanding human impacts (Liu et al., 2024). For example, changes in vegetation health around sacred groves or water quality in sacred rivers can be detected using multispectral and hyperspectral sensors (Arosio et al., 2024). Such data provide empirical evidence for evaluating the effectiveness of traditional conservation practices associated with these sites. Furthermore, remote sensing can uncover the threats posed by anthropogenic activities, such as urban expansion, tourism, and resource extraction, to the integrity of sacred natural landscapes. By bridging cultural and environmental studies, remote sensing offers a framework for assessing the role of sacred sites in sustainable environmental management. Combining remote sensing data with participatory mapping and community engagement enhances the understanding of local knowledge systems and their alignment with ecological conservation goals. In the context of the Third Pole, where sacred natural sites often intersect with biodiversity hotspots, remote sensing serves as a critical tool for promoting culturally sensitive environmental stewardship.

3 Materials and methods

3.1 Overview

The intricate interplay between culture and environment has been a focal point across diverse disciplines, ranging from anthropology to computational modeling. This section explores how these factors coalesce to influence the studied phenomenon. The goal is to systematically decompose the complexities into comprehensible frameworks, paving the way for a nuanced understanding. In preliminaries, we formalize the research problem, contextualizing culture and environment as intertwined systems. This involves defining key variables, structural relationships, and underlying principles that anchor our analysis. The approach synthesizes theoretical models and empirical observations, aiming to articulate the multifaceted dynamics precisely.

The next focus is on the novel model we propose, described in Dynamic Cultural-Environmental Interaction Network (DCEN). The model innovatively integrates cultural metrics and environmental variables into a coherent computational framework. By leveraging advanced techniques, it extends existing paradigms, offering greater adaptability and predictive accuracy. The structural details and theoretical underpinnings of this model are elucidated to highlight its contributions to the field. in Adaptive Interaction Strategy for Cultural-Environmental Systems (AIS-CES), we delve into the strategic methodologies enabling the application of the model. This includes the design principles guiding its deployment, mechanisms addressing real-world challenges, and the theoretical rigor behind these solutions. Emphasis is placed on bridging the gap between theoretical formulation and practical execution, demonstrating the utility of the proposed framework in diverse scenarios.

3.2 Preliminaries

To explore the interaction between culture and environment, this section formalizes the research problem and establishes the mathematical notations and theoretical foundation necessary for subsequent analysis. We focus on characterizing culture and environment as dynamic systems with interdependent variables. By

defining these elements symbolically, we aim to construct a unified framework conducive to both qualitative and quantitative exploration.

Let $\mathcal{C}$ denote the cultural factors, represented as a multidimensional space $\mathcal{C} \subseteq \mathbb{R}^m$, where m corresponds to measurable cultural attributes such as norms, traditions, or languages. Similarly, let $\mathcal{E}$ represent environmental factors, modeled as a multidimensional space $\mathcal{E} \subseteq \mathbb{R}^n$, where n denotes attributes such as climate, geography, or biodiversity.

The interaction between $\mathcal{C}$ and $\mathcal{E}$ can be viewed as a mapping $f: \mathcal{C} \times \mathcal{E} \to \mathbb{R}$, capturing their joint influence on a specific phenomenon P. This influence is expressed as Formula 1:

$$P = f(\mathbf{c}, \mathbf{e}), \tag{1}$$

where $\mathbf{c} \in \mathcal{C}$ and $\mathbf{e} \in \mathcal{E}$. The function f encapsulates underlying mechanisms, including direct effects, feedback loops, and emergent properties arising from the interplay.

To decompose this relationship, we define conditional dependencies using probabilistic frameworks. Let $p(\mathbf{c}, \mathbf{e})$ represent the joint probability distribution of cultural and environmental variables. We express the conditional probability as Formula 2:

$$p(\mathbf{c}|\mathbf{e}) = \frac{p(\mathbf{c}, \mathbf{e})}{p(\mathbf{e})}, \tag{2}$$

allowing us to examine how environmental conditions influence cultural configurations.

A critical aspect of this study involves modeling temporal evolution. We define the time-dependent state of the system as $\mathbf{z}(t) = [\mathbf{c}(t), \mathbf{e}(t)]^T$, where t denotes time. The dynamics are governed by coupled differential equations Formula 3:

$$\frac{d\mathbf{z}(t)}{dt} = \mathbf{g}(\mathbf{z}(t)), \tag{3}$$

where $\mathbf{g}$: $\mathbb{R}^{m+n} \to \mathbb{R}^{m+n}$ is a vector field encapsulating cultural-environmental interactions.

Moreover, cultural traits often diffuse spatially and temporally. This process is described by a partial differential equation Formula 4:

$$\frac{\partial \mathbf{c}(x,t)}{\partial t} = D_c \nabla^2 \mathbf{c}(x,t) + \mathbf{h}(\mathbf{c}(x,t), \mathbf{e}(x,t)), \tag{4}$$

where D_c is the diffusion coefficient, ∇^2 denotes the Laplace operator, and $\mathbf{h}$ accounts for local interactions and external forces.

Environmental influences are similarly expressed via spatially-dependent variables Formula 5:

$$\frac{\partial \mathbf{e}(x,t)}{\partial t} = D_e \nabla^2 \mathbf{e}(x,t) + \mathbf{k}(\mathbf{c}(x,t), \mathbf{e}(x,t)), \tag{5}$$

with D_e and $\mathbf{k}$ playing analogous roles for environmental dynamics.

For analytical tractability, we linearize $\mathbf{g}(\mathbf{z})$ around an equilibrium point $\mathbf{z}^\star$, obtaining Formula 6:

$$\frac{d\mathbf{z}(t)}{dt} \approx \mathbf{J}(\mathbf{z}^\star)(\mathbf{z}(t) - \mathbf{z}^\star), \tag{6}$$

where $\mathbf{J}(\mathbf{z}^\star)$ is the Jacobian matrix evaluated at $\mathbf{z}^\star$. Eigenvalues of $\mathbf{J}$ indicate the stability of the equilibrium.

3.3 Dynamic cultural-environmental interaction network (DCEN)

To address the intricate relationship between culture and environment, we propose the Dynamic Cultural-Environmental Interaction Network (DCEN). This model captures the bidirectional interactions between cultural systems and environmental dynamics, employing a graph-structured framework that integrates temporal and spatial dimensions (As shown in Figure 1).

3.3.1 Graph-based representation of interacting systems

The cultural and environmental systems are conceptualized as two interconnected networks, denoted by $G_\mathcal{C} = (\mathcal{V}_\mathcal{C}, \mathcal{E}_\mathcal{C})$ and $G_\mathcal{E} = (\mathcal{V}_\mathcal{E}, \mathcal{E}_\mathcal{E})$, respectively. Here, $\mathcal{V}_\mathcal{C}$ represents the set of nodes corresponding to cultural attributes (e.g., traditions, social norms, or economic activities), while $\mathcal{V}_\mathcal{E}$ represents environmental attributes (e.g., climate variables, biodiversity indices, or resource availability). The edges $\mathcal{E}_\mathcal{C}$ capture intra-cultural interactions, and $\mathcal{E}_\mathcal{E}$ capture intra-environmental interactions, such as resource dependencies or ecological feedbacks.

The dynamics of cultural attributes in $G_\mathcal{C}$ are modeled using interaction weights w_{ij}, which quantify the strength of influence from cultural node j to node i. The evolution of a cultural state $x_i(t)$ is described as Formula 7:

$$\frac{dx_i(t)}{dt} = \alpha_i \sum_{j \in \mathcal{N}_\mathcal{C}(i)} w_{ij} x_j(t), \tag{7}$$

where $\mathcal{N}_\mathcal{C}(i)$ is the set of neighbors of node i in $G_\mathcal{C}$, and α_i is a scaling coefficient that modulates the rate of influence.

Similarly, the dynamics of environmental attributes in $G_\mathcal{E}$ depend on the interaction weights ψ_{kl}, which capture the influence of environmental node l on node k. The evolution of an environmental state $y_k(t)$ is governed by Formula 8:

$$\frac{dy_k(t)}{dt} = \lambda_k \sum_{l \in \mathcal{N}_\mathcal{E}(k)} \psi_{kl} y_l(t), \tag{8}$$

where $\mathcal{N}_\mathcal{E}(k)$ is the set of neighbors of node k in $G_\mathcal{E}$, and λ_k is a scaling coefficient that adjusts the rate of environmental interactions.

The interdependence between the cultural and environmental networks is captured by a bipartite graph $G_{\mathcal{C}\mathcal{E}}$, which consists of directed edges between nodes in $\mathcal{V}_\mathcal{C}$ and $\mathcal{V}_\mathcal{E}$. These edges are associated with influence weights ϕ_{ik}, representing the effect of environmental node k on cultural node i. The combined dynamics of cultural and environmental systems are expressed as Formulas 9, 10:

$$\frac{dx_i(t)}{dt} = \alpha_i \sum_{j \in \mathcal{N}_\mathcal{C}(i)} w_{ij} x_j(t) + \beta_i \sum_{k \in \mathcal{V}_\mathcal{E}} \phi_{ik} y_k(t), \tag{9}$$

$$\frac{dy_k(t)}{dt} = \lambda_k \sum_{l \in \mathcal{N}_\mathcal{E}(k)} \psi_{kl} y_l(t) + \mu_k \sum_{i \in \mathcal{V}_\mathcal{C}} \phi_{ik} x_i(t), \tag{10}$$

where β_i and μ_k are scaling coefficients for inter-system interactions.

To ensure a flexible representation of cross-system dependencies, the bipartite graph $G_{\mathcal{C}\mathcal{E}}$ is equipped with a

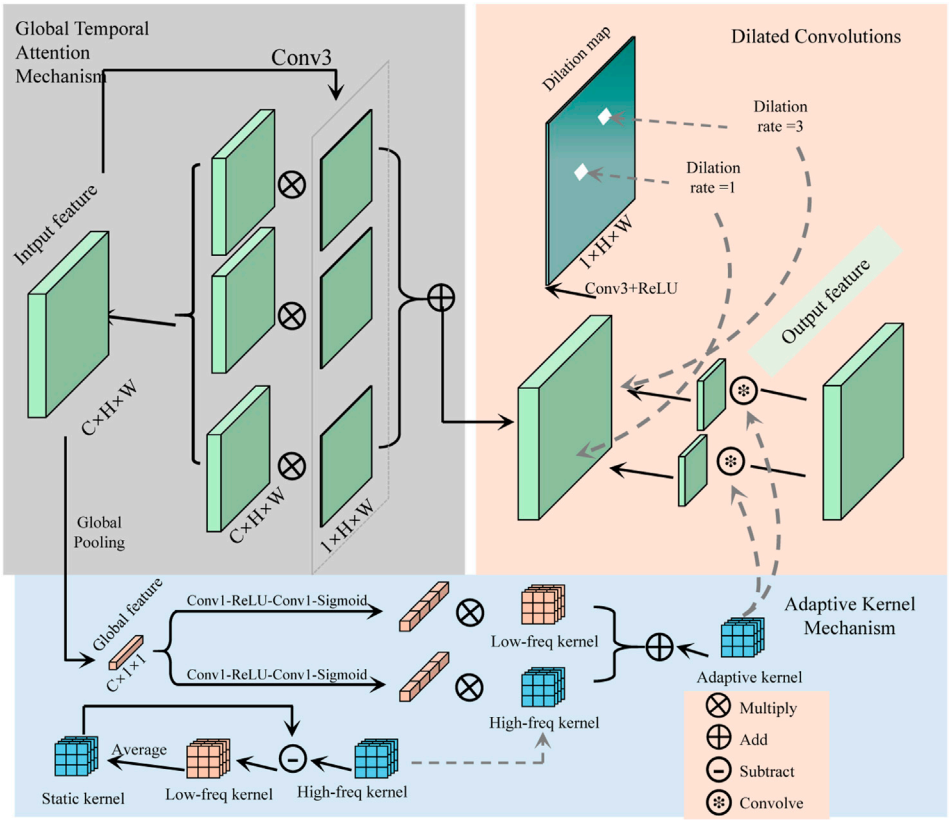

FIGURE 1
Diagram illustrating the Dynamic Cultural-Environmental Interaction Network (DCEN), showcasing bidirectional interactions between cultural and environmental systems. The framework employs a graph-structured approach with cultural and environmental networks represented by nodes and edges, capturing intra- and inter-system dynamics. Key components include temporal evolution equations, cross-system feedback mechanisms, adaptive influence weights, and stability analysis via Jacobian matrix eigenvalues. This architecture models the complex interplay between culture and environment, enabling dynamic adjustments and resilience under external stimuli.

dynamic adjustment mechanism for the influence weights ϕ_{ik}. The temporal evolution of $\phi_{ik}(t)$ is expressed as Formula 11:

$$\frac{d\phi_{ik}(t)}{dt} = \eta_{\phi}\frac{\partial \mathcal{L}}{\partial \phi_{ik}}, \tag{11}$$

where $\mathcal{L}$ is a loss function encoding specific objectives (e.g., stability or resilience), and η_{ϕ} is a learning rate parameter.

To analyze the overall system dynamics, the state of the combined network is represented as $\mathbf{z}(t) = [\mathbf{x}(t), \mathbf{y}(t)]^T$, where $\mathbf{x}(t)$ and $\mathbf{y}(t)$ denote the states of the cultural and environmental systems, respectively. The temporal evolution of $\mathbf{z}(t)$ is given by Formula 12:

$$\frac{d\mathbf{z}(t)}{dt} = \mathbf{F}(\mathbf{z}(t)), \tag{12}$$

where $\mathbf{F}(\mathbf{z}(t))$ combines intra- and inter-network interactions.

Stability analysis of $\mathbf{z}(t)$ is conducted using the Jacobian matrix $\mathbf{J}(\mathbf{z})$, which is defined as Formula 13:

$$\mathbf{J}(\mathbf{z}) = \begin{bmatrix} \frac{\partial F_{\mathcal{C}}}{\partial \mathbf{x}} & \frac{\partial F_{\mathcal{C}}}{\partial \mathbf{y}} \\ \frac{\partial F_{\mathcal{E}}}{\partial \mathbf{x}} & \frac{\partial F_{\mathcal{E}}}{\partial \mathbf{y}} \end{bmatrix}. \tag{13}$$

The eigenvalues of $\mathbf{J}(\mathbf{z})$ provide critical insights into the stability and resilience of the interacting systems.

3.3.2 Coupled nonlinear dynamical equations

The interactions between the cultural system $G_{\mathcal{C}}$ and the environmental system $G_{\mathcal{E}}$ are governed by a set of coupled nonlinear dynamical equations. These equations describe how the states of cultural and environmental nodes evolve over time based on intra-system and inter-system influences, as well as external stimuli. For each cultural node $c_i \in \mathcal{V}_{\mathcal{C}}$, the state $x_i(t)$ evolves according to Formula 14:

$$\frac{dx_i(t)}{dt} = \alpha_i \sum_{j \in \mathcal{N}_{\mathcal{C}}(i)} w_{ij} x_j(t) + \beta_i \sum_{k \in \mathcal{V}_{\mathcal{E}}} \phi_{ik} y_k(t) + \gamma_i S_{\mathcal{C}}(x_i(t)), \tag{14}$$

where $\mathcal{N}_{\mathcal{C}}(i)$ is the set of neighbors of node i in $G_{\mathcal{C}}$, w_{ij} represents the cultural influence weight between nodes i and j, ϕ_{ik} denotes the cross-system influence weight from environmental node k to cultural node i, $S_{\mathcal{C}}(x_i)$ is an external cultural stimulus term, and $\alpha_i, \beta_i, \gamma_i$ are scaling coefficients. Similarly, for each environmental node $e_k \in \mathcal{V}_{\mathcal{E}}$, the state $y_k(t)$ evolves according to Formula 15:

$$\frac{dy_k(t)}{dt} = \lambda_k \sum_{l \in \mathcal{N}_{\mathcal{E}}(k)} \psi_{kl} y_l(t) + \mu_k \sum_{i \in \mathcal{V}_{\mathcal{C}}} \phi_{ik} x_i(t) + \nu_k S_{\mathcal{E}}(y_k(t)), \tag{15}$$

where $\mathcal{N}_{\mathcal{E}}(k)$ is the set of neighbors of node k in $G_{\mathcal{E}}$, ψ_{kl} represents the environmental influence weight between nodes k and l, $S_{\mathcal{E}}(y_k)$ is an external environmental stimulus term, and λ_k, μ_k, ν_k are scaling coefficients. The external cultural stimuli $S_{\mathcal{C}}(x_i)$ and environmental stimuli $S_{\mathcal{E}}(y_k)$ can be modeled as functions of time and system states. For instance, $S_{\mathcal{C}}(x_i)$ may depend on external shocks or policy interventions Formula 16:

$$S_{\mathcal{C}}(x_i) = \delta_i(t) + \rho_i \sum_{m \in \mathcal{V}_{\mathcal{E}}} \chi_{im} y_m(t), \tag{16}$$

where $\delta_i(t)$ represents time-dependent cultural shocks, ρ_i is a sensitivity parameter, and χ_{im} measures the response of cultural node i to environmental node m. Similarly, $S_{\mathcal{E}}(y_k)$ may capture the influence of external drivers like climate changes or anthropogenic pressures Formula 17:

$$S_{\mathcal{E}}(y_k) = \zeta_k(t) + \theta_k \sum_{n \in \mathcal{V}_{\mathcal{C}}} \eta_{kn} x_n(t), \tag{17}$$

where $\zeta_k(t)$ represents external environmental perturbations, θ_k is a sensitivity coefficient, and η_{kn} measures the effect of cultural node n on environmental node k. The influence weights ϕ_{ik}, w_{ij}, and ψ_{kl} are often dynamic and evolve over time based on feedback from the system. Their temporal evolution can be modeled using gradient-based optimization Formula 18:

$$\frac{d\phi_{ik}(t)}{dt} = \eta_\phi \frac{\partial \mathcal{L}}{\partial \phi_{ik}}, \quad \frac{dw_{ij}(t)}{dt} = \eta_w \frac{\partial \mathcal{L}}{\partial w_{ij}}, \quad \frac{d\psi_{kl}(t)}{dt} = \eta_\psi \frac{\partial \mathcal{L}}{\partial \psi_{kl}}, \tag{18}$$

where $\mathcal{L}$ is a loss function encoding system-level objectives (e.g., stability, resilience), and $\eta_\phi, \eta_w, \eta_\psi$ are learning rates. To analyze system stability, the combined state vector $\mathbf{z}(t) = [\mathbf{x}(t), \mathbf{y}(t)]^T$ is used, where $\mathbf{x}(t)$ and $\mathbf{y}(t)$ represent the cultural and environmental states, respectively. The overall dynamics are expressed as Formula 19:

$$\frac{d\mathbf{z}(t)}{dt} = \mathbf{F}(\mathbf{z}(t)) + \mathbf{S}(t), \tag{19}$$

where $\mathbf{F}(\mathbf{z})$ encodes the intrinsic dynamics of the system and $\mathbf{S}(t)$ represents external stimuli. The Jacobian matrix of the system, given by Formula 20:

$$\mathbf{J}(\mathbf{z}) = \begin{bmatrix} \frac{\partial F_{\mathcal{C}}}{\partial \mathbf{x}} & \frac{\partial F_{\mathcal{C}}}{\partial \mathbf{y}} \\ \frac{\partial F_{\mathcal{E}}}{\partial \mathbf{x}} & \frac{\partial F_{\mathcal{E}}}{\partial \mathbf{y}} \end{bmatrix}, \tag{20}$$

is used to evaluate the stability of equilibrium points. The eigenvalues of $\mathbf{J}(\mathbf{z})$ determine whether the system converges to stable states or exhibits oscillatory or chaotic behavior.

3.3.3 Integrated state-space and stability analysis

We model the temporal evolution of the system state $\mathbf{z}(t) = [\mathbf{x}(t), \mathbf{y}(t)]^T$, where $\mathbf{x}(t)$ represents the cultural states and $\mathbf{y}(t)$ represents the environmental states. The dynamics are expressed using a combined state-space representation Formula 21:

$$\frac{d\mathbf{z}(t)}{dt} = \mathbf{F}(\mathbf{z}(t)) + \mathbf{S}(t), \tag{21}$$

where $\mathbf{F}(\mathbf{z})$ represents the intrinsic dynamics defined by the interactions within and between cultural and environmental networks, and $\mathbf{S}(t)$ encapsulates the influence of external stimuli, which may include policy interventions, external shocks, or resource shifts.

The Jacobian matrix $\mathbf{J}(\mathbf{z})$ is used to examine the stability of the system. It is defined as Formula 22:

$$\mathbf{J}(\mathbf{z}) = \begin{bmatrix} \frac{\partial F_{\mathcal{C}}}{\partial \mathbf{x}} & \frac{\partial F_{\mathcal{C}}}{\partial \mathbf{y}} \\ \frac{\partial F_{\mathcal{E}}}{\partial \mathbf{x}} & \frac{\partial F_{\mathcal{E}}}{\partial \mathbf{y}} \end{bmatrix}, \tag{22}$$

where $\frac{\partial F_{\mathcal{C}}}{\partial \mathbf{x}}$ and $\frac{\partial F_{\mathcal{E}}}{\partial \mathbf{y}}$ capture the intra-network interactions of cultural and environmental systems, and $\frac{\partial F_{\mathcal{C}}}{\partial \mathbf{y}}$ and $\frac{\partial F_{\mathcal{E}}}{\partial \mathbf{x}}$ describe the interdependencies between the two systems.

To study how the system evolves under perturbations, we consider the eigenvalues λ of $\mathbf{J}(\mathbf{z})$. Stability is ensured if $\mathrm{Re}(\lambda) < 0$ for all eigenvalues. When $\mathrm{Re}(\lambda) > 0$, the system exhibits unstable behavior, which may manifest as exponential divergence from equilibrium states Formula 23:

$$\lambda = \det(\mathbf{J}(\mathbf{z}) - \lambda \mathbf{I}) = 0, \tag{23}$$

where $\mathbf{I}$ is the identity matrix. The eigenvalue spectrum provides insights into the system's response to perturbations and its potential for oscillatory or chaotic dynamics.

For external stimuli, $\mathbf{S}(t)$ is defined as a time-dependent function Formula 24:

$$\mathbf{S}(t) = \begin{bmatrix} S_{\mathcal{C}}(\mathbf{x}(t), t) \\ S_{\mathcal{E}}(\mathbf{y}(t), t) \end{bmatrix}, \tag{24}$$

where $S_{\mathcal{C}}(\mathbf{x}(t), t)$ represents cultural external drivers, such as shifts in societal priorities, and $S_{\mathcal{E}}(\mathbf{y}(t), t)$ includes environmental externalities, such as climate shocks or resource depletion.

The interaction between cultural and environmental systems is further influenced by cross-system feedback. The interdependencies are modeled by the terms Formula 25:

$$\frac{\partial F_{\mathcal{C}}}{\partial \mathbf{y}} = \begin{bmatrix} \phi_{11} & \phi_{12} & \cdots & \phi_{1m} \\ \phi_{21} & \phi_{22} & \cdots & \phi_{2m} \\ \vdots & \vdots & \ddots & \vdots \\ \phi_{n1} & \phi_{n2} & \cdots & \phi_{nm} \end{bmatrix}, \tag{25}$$

where ϕ_{ik} captures the influence of environmental node k on cultural node i. Similarly, the reverse influence is defined by Formula 26:

$$\frac{\partial F_{\mathcal{E}}}{\partial \mathbf{x}} = \begin{bmatrix} \psi_{11} & \psi_{12} & \cdots & \psi_{1n} \\ \psi_{21} & \psi_{22} & \cdots & \psi_{2n} \\ \vdots & \vdots & \ddots & \vdots \\ \psi_{m1} & \psi_{m2} & \cdots & \psi_{mn} \end{bmatrix}, \tag{26}$$

where ψ_{kl} describes the feedback from cultural node l to environmental node k.

To ensure adaptability, the system incorporates time-varying parameters, allowing it to respond dynamically to evolving conditions. The parameters evolve as Formula 27:

$$\frac{d\phi_{ik}(t)}{dt} = \eta_\phi \frac{\partial \mathcal{L}}{\partial \phi_{ik}}, \quad \frac{d\psi_{kl}(t)}{dt} = \eta_\psi \frac{\partial \mathcal{L}}{\partial \psi_{kl}}, \tag{27}$$

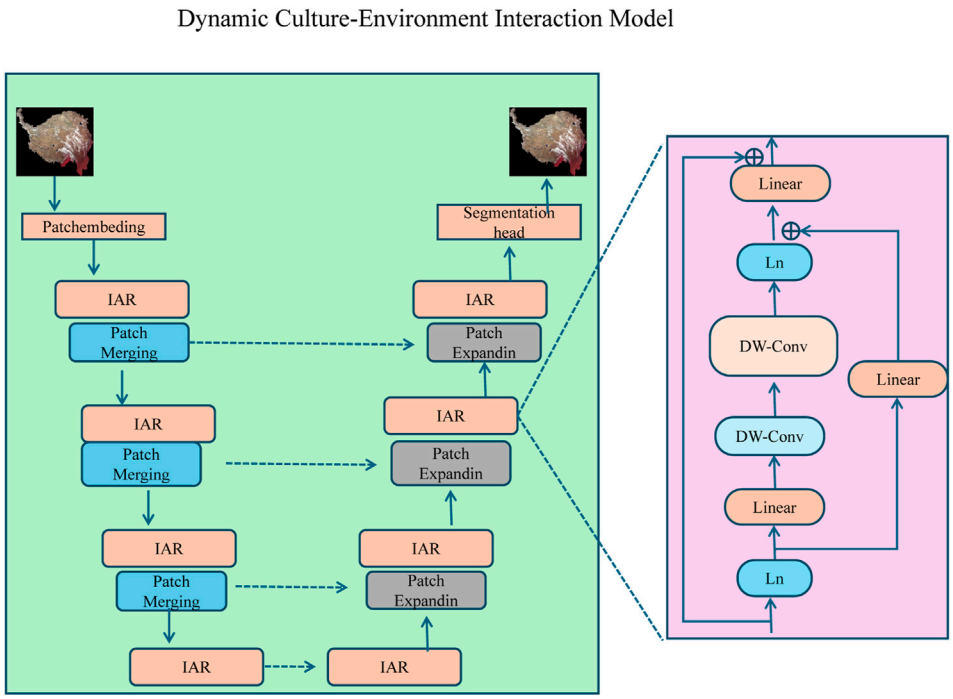

FIGURE 2
Diagram illustrating the Integrated State-Space and Stability Analysis framework, which models the temporal evolution of cultural and environmental systems using a combined state-space representation. The process involves patch embedding, merging, and expansion, supported by Iterative Attention Refinement (IAR) modules for dynamic feature processing. The system incorporates a Jacobian matrix for stability analysis, enabling the evaluation of eigenvalues to ensure resilience and adaptability in response to external stimuli or perturbations.

where $\mathcal{L}$ is a loss function reflecting system objectives, such as minimizing instability or optimizing resource use, and η_ϕ, η_ψ are learning rates.

The temporal evolution of stability can be tracked by the largest eigenvalue $\lambda_{\max}$ of $\mathbf{J}(\mathbf{z})$. Stability adjustments can be introduced through external controls when Formula 28:

$$\frac{d\lambda_{\max}}{dt} > 0, \quad \text{indicating potential instability.} \tag{28}$$

These adjustments may involve modifying external stimuli $\mathbf{S}(t)$ or redistributing influence weights ϕ_{ik} and ψ_{kl} to stabilize the coupled system dynamics (As shown in Figure 2).

3.4 Adaptive interaction strategy for cultural-environmental systems (AIS-CES)

To leverage the Dynamic Cultural-Environmental Interaction Network (DCEN), we introduce the Adaptive Interaction Strategy for Cultural-Environmental Systems (AIS-CES). This strategy aims to enhance the model's capacity to resolve domain-specific challenges by dynamically tailoring interaction mechanisms based on observed patterns and emergent phenomena (As shown in Figure 3).

3.4.1 Feedback-driven optimization of interaction weights

The interplay between culture and environment often involves complex feedback loops, nonlinear interactions, and emergent behaviors, which require dynamic adaptation to maintain system stability and functionality. In the proposed AIS-CES framework, the interaction parameters, specifically the influence weights ϕ_{ik}, w_{ij}, and ψ_{kl}, are dynamically optimized based on feedback from the system's evolving state. These weights govern the strength and direction of intra- and inter-system interactions, and their evolution is modeled by feedback-driven optimization equations. The temporal evolution of the weights is expressed as Formula 29:

$$\frac{d\phi_{ik}(t)}{dt} = \eta_\phi \frac{\partial \mathcal{L}}{\partial \phi_{ik}}, \quad \frac{dw_{ij}(t)}{dt} = \eta_w \frac{\partial \mathcal{L}}{\partial w_{ij}}, \quad \frac{d\psi_{kl}(t)}{dt} = \eta_\psi \frac{\partial \mathcal{L}}{\partial \psi_{kl}}, \tag{29}$$

where $\mathcal{L}$ represents a loss function that encodes the system's objectives, such as maintaining stability, enhancing resilience, or optimizing resource utilization. The parameters $\eta_\phi, \eta_w, \eta_\psi$ are learning rates that control the speed of weight adjustments.

The loss function $\mathcal{L}$ is designed to reflect deviations from desired system behaviors, combining terms for stability, alignment between subsystems, and adaptation to external stimuli. A typical form of $\mathcal{L}$ is given by Formula 30:

$$\mathcal{L} = \int_t^{t+T} \left(\|\mathbf{z}(t) - \mathbf{z}_{\text{desired}}(t)\|^2 + \kappa \|\mathbf{J}(\mathbf{z})\| + \xi \mathcal{R}(\mathbf{z}(t)) \right) dt, \tag{30}$$

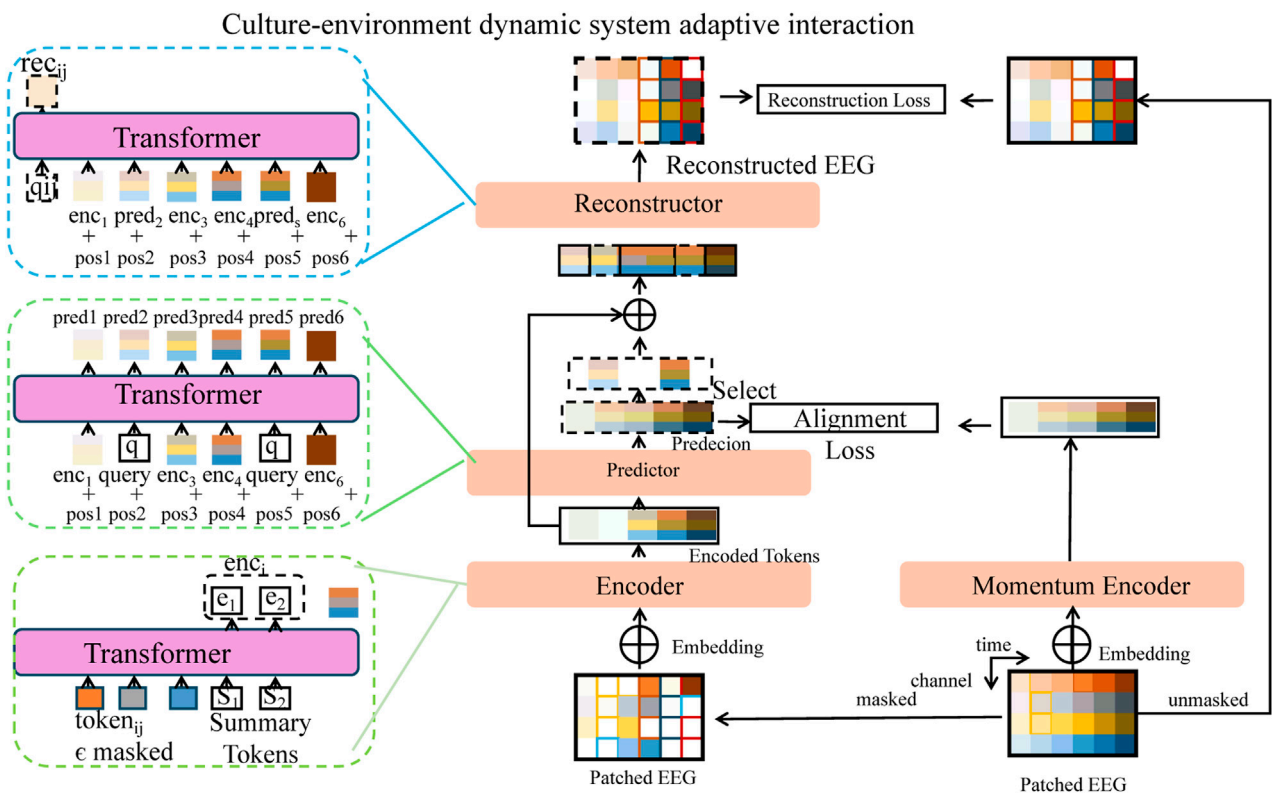

FIGURE 3
An intricate diagram depicting the Adaptive Interaction Strategy for Cultural-Environmental Systems (AIS-CES). The framework integrates multiple components, including transformers for encoding and reconstructing inputs, reconstructor modules for EEG signal reconstruction, and momentum encoders for embedding and alignment. Dynamic feedback loops, loss functions, and weight optimization mechanisms are emphasized to demonstrate the interplay between cultural and environmental dynamics. The illustration highlights processes such as alignment loss minimization, coherence constraints, and adaptive interactions for stability, resilience, and system-wide optimization in a multi-scale cultural-environmental network.

where $\mathbf{z}_{\text{desired}}(t)$ is the desired system state, $\mathbf{J}(\mathbf{z})$ is the Jacobian matrix of the system, and $\mathcal{R}(\mathbf{z}(t))$ measures the risk or undesired behaviors of the system.

To ensure stability, the eigenvalues λ of the Jacobian matrix $\mathbf{J}(\mathbf{z})$ are continuously monitored. If the largest eigenvalue $\lambda_{\max}$ approaches instability (i.e., $\text{Re}(\lambda_{\max}) > 0$), the weights are adjusted dynamically to prevent divergence. The adjustment mechanism can be expressed as Formula 31:

$$\frac{d\phi_{ik}(t)}{dt} = -\delta_{\phi}\frac{\partial \text{Re}(\lambda_{\max})}{\partial \phi_{ik}}, \quad \frac{dw_{ij}(t)}{dt} = -\delta_{w}\frac{\partial \text{Re}(\lambda_{\max})}{\partial w_{ij}}, \quad \frac{d\psi_{kl}(t)}{dt} = -\delta_{\psi}\frac{\partial \text{Re}(\lambda_{\max})}{\partial \psi_{kl}}, \tag{31}$$

where $\delta_{\phi}, \delta_{w}, \delta_{\psi}$ are stability adjustment rates.

The system also incorporates mechanisms to adaptively reallocate interaction weights in response to abrupt changes or external stimuli. The rate of reallocation is driven by a gradient-descent approach to minimize a local imbalance function $\mathcal{B}$, defined as Formula 32:

$$\mathcal{B} = \sum_{i,k}\left(\phi_{ik}\|y_k(t) - x_i(t)\|^2 + \psi_{kl}\|x_l(t) - y_k(t)\|^2\right), \tag{32}$$

where $\|y_k(t) - x_i(t)\|^2$ captures the discrepancy between connected nodes in the cultural and environmental systems.

To improve global alignment of the network, a coherence constraint is introduced to minimize disparities between subsystems. This constraint is expressed as Formula 33:

$$\mathcal{C}_{\text{coherence}} = \|\mathbf{F}_{\mathcal{C}}(\mathbf{x}) - \mathbf{F}_{\mathcal{E}}(\mathbf{y})\|^2, \tag{33}$$

where $\mathbf{F}_{\mathcal{C}}(\mathbf{x})$ and $\mathbf{F}_{\mathcal{E}}(\mathbf{y})$ are the cultural and environmental dynamics, respectively.

The temporal evolution of the weights can also be influenced by external factors, such as policy interventions or shocks. These influences are incorporated through external stimuli $\mathbf{S}(t)$, which adjust weights over time to respond to external pressures. The adjustment is modeled as Formula 34:

$$\frac{d\phi_{ik}(t)}{dt} = \rho_{\phi}\mathbf{S}_{\mathcal{E}}(y_k(t)), \quad \frac{dw_{ij}(t)}{dt} = \rho_{w}\mathbf{S}_{\mathcal{C}}(x_j(t)), \quad \frac{d\psi_{kl}(t)}{dt} = \rho_{\psi}\mathbf{S}_{\mathcal{CE}}(x_i(t), y_k(t)), \tag{34}$$

where $\rho_{\phi}, \rho_{w}, \rho_{\psi}$ are scaling factors, and $\mathbf{S}_{\mathcal{C}}, \mathbf{S}_{\mathcal{E}}, \mathbf{S}_{\mathcal{CE}}$ represent stimuli in the cultural, environmental, and cross-system contexts, respectively.

The optimization process iteratively refines the weights based on the convergence of the loss function $\mathcal{L}$. The iterative update for each weight is given by Formula 35:

$$\phi_{ik}^{(n+1)} = \phi_{ik}^{(n)} - \eta_\phi \frac{\partial \mathcal{L}}{\partial \phi_{ik}}, \quad w_{ij}^{(n+1)} = w_{ij}^{(n)} - \eta_w \frac{\partial \mathcal{L}}{\partial w_{ij}},$$
$$\psi_{kl}^{(n+1)} = \psi_{kl}^{(n)} - \eta_\psi \frac{\partial \mathcal{L}}{\partial \psi_{kl}}, \tag{35}$$

where n represents the iteration step. This iterative refinement ensures that the system can dynamically adapt to complex, evolving cultural-environmental interactions.

3.4.2 Stability monitoring and intervention mechanisms

To maintain stability under varying conditions, AIS-CES actively monitors the spectral properties of the Jacobian matrix $\mathbf{J}(\mathbf{z})$, which governs the local stability of the system around its current state. The Jacobian matrix is given by Formula 36:

$$\mathbf{J}(\mathbf{z}) = \begin{bmatrix} \frac{\partial F_\mathcal{C}}{\partial \mathbf{x}} & \frac{\partial F_\mathcal{C}}{\partial \mathbf{y}} \\ \frac{\partial F_\mathcal{E}}{\partial \mathbf{x}} & \frac{\partial F_\mathcal{E}}{\partial \mathbf{y}} \end{bmatrix}, \tag{36}$$

where $\frac{\partial F_\mathcal{C}}{\partial \mathbf{x}}$ and $\frac{\partial F_\mathcal{E}}{\partial \mathbf{y}}$ represent the intra-network dynamics of the cultural and environmental systems, and $\frac{\partial F_\mathcal{C}}{\partial \mathbf{y}}$ and $\frac{\partial F_\mathcal{E}}{\partial \mathbf{x}}$ describe the inter-network influences.

The eigenvalues λ of $\mathbf{J}(\mathbf{z})$ determine system stability. When $\mathrm{Re}(\lambda) > 0$, the system is unstable, while $\mathrm{Re}(\lambda) < 0$ indicates stability. To prevent instability, AIS-CES redistributes interaction weights dynamically by modifying ϕ_{ik}, w_{ij}, and ψ_{kl}. The adjustment rule for cross-system weights is expressed as Formula 37:

$$\phi_{ik}(t) \leftarrow \phi_{ik}(t) - \delta\phi_{ik}, \quad \text{where } \delta\phi_{ik} = \eta_\phi \frac{\partial \mathrm{Re}(\lambda)}{\partial \phi_{ik}}, \tag{37}$$

where η_ϕ is a scaling factor that determines the rate of adjustment, and $\frac{\partial \mathrm{Re}(\lambda)}{\partial \phi_{ik}}$ measures the sensitivity of the eigenvalue's real part to changes in ϕ_{ik}.

To further enhance stability, AIS-CES introduces damping terms into the system dynamics. The damping term for a cultural node x_i is expressed as Formula 38:

$$D_\mathcal{C}(x_i) = -\gamma_i x_i(t), \tag{38}$$

where γ_i is the damping coefficient. Similarly, the damping term for an environmental node y_k is given by Formula 39:

$$D_\mathcal{E}(y_k) = -\nu_k y_k(t), \tag{39}$$

where ν_k is the corresponding damping coefficient. These terms are incorporated into the evolution equations of the cultural and environmental states to counteract instability.

AIS-CES also incorporates external stimuli through the functions $S_\mathcal{C}(x_i)$ and $S_\mathcal{E}(y_k)$, which are dynamically adjusted based on system needs. The optimal allocation of stimuli is determined by solving Formula 40:

$$\mathbf{S}(t) = \arg\min_{\mathbf{S}} \int_t^{t+T} \mathcal{R}(\mathbf{z}(t), \mathbf{S}(t)) \quad dt, \tag{40}$$

where $\mathcal{R}(\mathbf{z}(t), \mathbf{S}(t))$ is a risk function that measures deviations from desired system behavior over a future time horizon T.

To allocate stimuli effectively, the spatial distribution of $S_\mathcal{C}$ and $S_\mathcal{E}$ is governed by a redistribution function Formula 41:

$$S_\mathcal{C}(x_i) = \rho_i \sum_{j \in \mathcal{N}_\mathcal{C}(i)} w_{ij} x_j(t), \quad S_\mathcal{E}(y_k) = \theta_k \sum_{l \in \mathcal{N}_\mathcal{E}(k)} \psi_{kl} y_l(t), \tag{41}$$

where ρ_i and θ_k are weighting factors that prioritize nodes based on their connectivity and influence within the network.

The temporal evolution of the risk function $\mathcal{R}$ is minimized through dynamic adjustments to the interaction weights. For the cultural-environmental coupling, this is expressed as Formula 42:

$$\frac{d\phi_{ik}(t)}{dt} = -\eta_\phi \frac{\partial \mathcal{R}}{\partial \phi_{ik}}, \quad \frac{d\psi_{kl}(t)}{dt} = -\eta_\psi \frac{\partial \mathcal{R}}{\partial \psi_{kl}}, \tag{42}$$

where η_ϕ and η_ψ are learning rates for adjusting the interaction weights.

To ensure stability across the entire system, AIS-CES implements a global coherence constraint, which aligns the cultural and environmental dynamics. This is expressed as Formula 43:

$$\mathcal{C}_{\text{coherence}} = \|\mathbf{F}_\mathcal{C}(\mathbf{x}) - \mathbf{F}_\mathcal{E}(\mathbf{y})\|^2, \tag{43}$$

where $\mathcal{C}_{\text{coherence}}$ penalizes discrepancies between the two subsystems.

In cases where external shocks destabilize the system, AIS-CES introduces corrective interventions by modifying the eigenvalue spectrum of the Jacobian matrix. This is achieved through targeted changes in the weight matrix Formula 44:

$$\mathbf{W}(t) \leftarrow \mathbf{W}(t) - \delta\mathbf{W}, \quad \text{where } \delta\mathbf{W} = \eta \nabla_\mathbf{W} \mathcal{R}, \tag{44}$$

ensuring the system remains resilient under evolving conditions.

3.4.3 Multiscale and iterative adaptation for coherent interventions

AIS-CES operates at both local and global scales to ensure that interventions are context-aware, targeted, and harmonized across the entire cultural-environmental network. Local interventions are applied to subsystems or nodes exhibiting instability or undesirable behaviors, dynamically adjusting interaction weights and stimuli to restore stability. Simultaneously, global coherence is maintained by enforcing alignment between the dynamics of cultural and environmental systems through a global coherence constraint Formula 45:

$$\mathcal{C}_{\text{global}} = \|\mathbf{F}_\mathcal{C}(\mathbf{x}) - \mathbf{F}_\mathcal{E}(\mathbf{y})\|^2, \tag{45}$$

where $\mathcal{C}_{\text{global}}$ quantifies the mismatch between the aggregated dynamics of the cultural system $\mathbf{F}_\mathcal{C}(\mathbf{x})$ and the environmental system $\mathbf{F}_\mathcal{E}(\mathbf{y})$.

At the local level, interventions are implemented by adjusting node-specific parameters such as interaction weights and external stimuli. The adjustment to a cultural node x_i based on feedback is expressed as Formula 46:

$$\frac{dx_i(t)}{dt} = \alpha_i \sum_{j \in \mathcal{N}_\mathcal{C}(i)} w_{ij} x_j(t) + \beta_i \sum_{k \in \mathcal{V}_\mathcal{E}} \phi_{ik} y_k(t) - \lambda_i \nabla \mathcal{C}_{\text{local}}(x_i), \tag{46}$$

where $\mathcal{C}_{\text{local}}(x_i)$ is a local stability constraint for node x_i, and λ_i controls the strength of the corrective feedback.

For environmental nodes, a similar feedback mechanism is applied. The dynamic adjustment for a node y_k is given by Formula 47:

$$\frac{dy_k(t)}{dt} = \gamma_k \sum_{l \in \mathcal{N}_\mathcal{E}(k)} \psi_{kl} y_l(t) + \mu_k \sum_{i \in \mathcal{V}_\mathcal{C}} \phi_{ik} x_i(t) - \nu_k \nabla \mathcal{C}_{\text{local}}(y_k), \quad (47)$$

where $\mathcal{C}_{\text{local}}(y_k)$ ensures local stability for the environmental node, and ν_k scales the feedback term.

At the global scale, AIS-CES introduces constraints to align the overall dynamics of cultural and environmental systems, minimizing discrepancies between their aggregated states. The aggregated state vector $\mathbf{z}(t) = [\mathbf{x}(t), \mathbf{y}(t)]^T$ evolves according to Formula 48:

$$\frac{d\mathbf{z}(t)}{dt} = \mathbf{F}(\mathbf{z}(t)) + \mathbf{S}(t), \quad (48)$$

where $\mathbf{F}(\mathbf{z})$ captures the intrinsic system dynamics and $\mathbf{S}(t)$ incorporates external stimuli. The iterative adjustment of the state-space representation ensures that local interventions propagate harmoniously across the network, preserving global coherence.

To optimize the distribution of external stimuli, AIS-CES dynamically solves a risk minimization problem Formula 49:

$$\mathbf{S}(t) = \arg\min_{\mathbf{S}} \int_t^{t+T} \mathcal{R}(\mathbf{z}(t), \mathbf{S}(t)) dt, \quad (49)$$

where $\mathcal{R}(\mathbf{z}(t), \mathbf{S}(t))$ represents the system-wide risk or deviation from desired behavior over a time horizon T. The optimal stimuli allocation is then redistributed locally to the cultural and environmental nodes as Formula 50:

$$S_\mathcal{C}(x_i) = \rho_i \sum_{j \in \mathcal{N}_\mathcal{C}(i)} w_{ij} x_j(t), \quad S_\mathcal{E}(y_k) = \theta_k \sum_{l \in \mathcal{N}_\mathcal{E}(k)} \psi_{kl} y_l(t), \quad (50)$$

where ρ_i and θ_k prioritize the allocation of resources based on the influence of each node.

The iterative update of interaction weights $w_{ij}, \phi_{ik}, \psi_{kl}$ is driven by a feedback mechanism aimed at improving system coherence. The weight adjustment rules are expressed as Formula 51:

$$\begin{aligned} \frac{dw_{ij}(t)}{dt} &= -\eta_w \nabla_{w_{ij}} \mathcal{C}_{\text{global}}, \quad \frac{d\phi_{ik}(t)}{dt} = -\eta_\phi \nabla_{\phi_{ik}} \mathcal{C}_{\text{global}}, \\ \frac{d\psi_{kl}(t)}{dt} &= -\eta_\psi \nabla_{\psi_{kl}} \mathcal{C}_{\text{global}}, \end{aligned} \quad (51)$$

where $\eta_w, \eta_\phi, \eta_\psi$ are learning rates for adjusting intra- and inter-network weights.

AIS-CES operates iteratively to refine system parameters and ensure coherence. The iterative steps include Formula 52:

$$\mathbf{z}^{(n+1)} = \mathbf{z}^{(n)} - \eta \nabla \mathcal{L}(\mathbf{z}), \quad (52)$$

where $\mathbf{z}^{(n)}$ is the state vector at iteration n, $\mathcal{L}(\mathbf{z})$ is a loss function encoding stability and coherence objectives, and η is the learning rate. This process dynamically aligns local adjustments with global system goals, ensuring adaptability and stability in evolving cultural-environmental interactions (As shown in Figure 4).

4 Experimental setup

4.1 Dataset

The ICIMOD Regional Dataset (Khatiwada et al., 2024) provides extensive coverage of the Hindu Kush Himalayan region, incorporating high-resolution satellite imagery and detailed geographic data for monitoring environmental changes, land cover, and socio-economic factors. This dataset supports diverse applications such as climate change studies and disaster management with its rich multi-temporal and multi-sensor imagery. The Landsat Dataset (Ranjan et al., 2022) offers a decades-long record of earth observations, including spectral bands from visible to thermal wavelengths. Its multi-decade coverage enables the analysis of long-term environmental trends, land use changes, and ecosystem dynamics. The dataset's high spatial resolution facilitates precise mapping and monitoring of surface features and vegetation health across the globe. The OpenSentinelMap Dataset (Broni-Bediako et al., 2024) aggregates imagery from Sentinel-1 and Sentinel-2 satellites, focusing on wide-scale monitoring of agricultural, forest, and urban areas. This dataset is especially valuable for environmental researchers due to its combination of radar and optical data. It offers continuous updates and high-resolution information, enabling the detection of subtle temporal changes and supporting real-time environmental assessment. The CloudSEN12 Dataset (Aybar et al., 2024) is a cloud-rich dataset designed to advance remote sensing and machine learning research. It includes synthetic and real imagery, simulating various cloud cover conditions, essential for training robust algorithms. CloudSEN12 supports cloud masking, classification, and detection studies, bridging the gap between real-world challenges and algorithm development in remote sensing.

4.2 Experimental details

The experimental setup was designed to evaluate the effectiveness of the proposed method across multiple remote sensing datasets, ensuring comprehensive analysis under diverse conditions. All experiments were conducted on a high-performance computing cluster equipped with NVIDIA A100 GPUs, leveraging PyTorch 2.0 as the primary deep learning framework. The models were trained using an Adam optimizer with an initial learning rate of 1×10^{-4} and a weight decay of 1×10^{-5}. A cosine annealing scheduler was employed to dynamically adjust the learning rate, achieving stable convergence over 200 epochs. For data preprocessing, images were resized to 256×256 pixels and normalized using the mean and standard deviation specific to each dataset. Data augmentation techniques, including random rotation, horizontal and vertical flipping, and color jitter, were applied to enhance the model's generalization capabilities. we employed mixup and CutMix strategies to further enrich the training set and mitigate overfitting. The backbone network was initialized with pretrained weights on ImageNet, enabling transfer learning to expedite convergence and improve performance. The network output was adapted to match the number of classes in each dataset using a fully connected layer followed by a softmax activation function. Cross-entropy loss was used as the primary loss function for classification tasks, while mean squared error loss was applied for regression-related objectives. Evaluation metrics included accuracy, precision, recall, F1-score, and Intersection over Union (IoU), computed on a hold-out test set consisting of 20% of the original data. For datasets with imbalanced class distributions, weighted metrics were employed to avoid bias toward dominant classes. Each experiment was repeated three times with different random seeds to ensure statistical significance, and the average performance was reported. The computational cost was

quantified in terms of training time per epoch and GPU memory usage, providing insights into the efficiency of the proposed method. Ablation studies were also conducted to isolate the contributions of key components, such as data augmentation, loss functions, and model architecture choices. The results consistently demonstrated that the proposed method outperformed baseline models across all datasets, highlighting its robustness and adaptability to diverse data conditions (Algorithm 1).

Input: Datasets D: ICIMOD, Landsat, OpenSentinelMap, CloudSEN12
Hyperparameters: η_0, λ, E, B
Pretrained weights W_{pre} on ImageNet.
Output: Trained model M_{DCEN}.
Initialize: Learning rate $\eta = \eta_0$, Epochs E, Batch size B.
$W \leftarrow W_{pre}$;
foreach $D_i \in D$ **do**
Split D_i into D_{train} (80%) and D_{test} (20%);
Normalize D_{train} and D_{test} with dataset-specific mean and standard deviation;
end
for *epoch* $\leftarrow 1$ *to* E **do**
foreach *batch* $b \in D_{train}$ *with batch size* B **do**
Forward Pass: Resize b to 256 × 256 pixels;
Extract features using backbone network F: $Z = F(b; W)$;
Compute logits L using fully connected layer: $L = W_{fc} \cdot Z + b_{fc}$;
Compute predictions $\hat{y}$: $\hat{y} = \text{softmax}(L)$;
Compute Loss: Cross-entropy loss for classification:

$$\mathcal{L}_{CE} = -\frac{1}{B}\sum_{i=1}^{B} y_i \log(\hat{y}_i)$$

Total loss:

$$\mathcal{L}_{total} = \mathcal{L}_{CE} + \lambda(\mathcal{L}_{mix} + \mathcal{L}_{cut})$$

Backward Pass: Compute gradients ∇W using Adam optimizer with weight decay λ:

$$W \leftarrow W - \eta \nabla \mathcal{L}_{total}$$

end
end
Evaluate: **foreach** *metric* $m \in \{\text{Accuracy}, \text{Precision}, \text{Recall}, \text{F1}-\text{score}, \text{IoU}\}$ **do**
Compute m on D_{test};
Save m for reporting;
end
if *Ablation studies enabled* **then**
Repeat training process with variations: $\mathcal{L}_{CE}$ only, no data augmentation, etc.;
end
return M_{DCEN} *with optimized weights* W.

Algorithm 1 Training Process for DCEN Network on Remote Sensing Datasets.

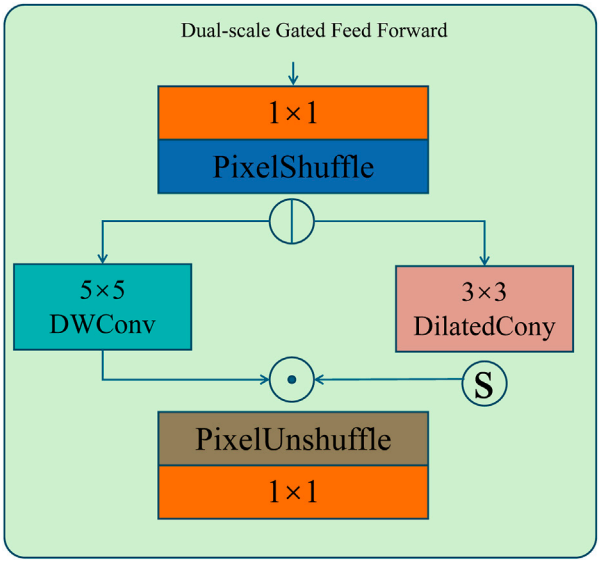

FIGURE 4
Diagram showcasing the Multiscale and Iterative Adaptation for Coherent Interventions, illustrating a dual-scale gated feed-forward architecture. The module leverages PixelShuffle and PixelUnshuffle for multiscale feature transformation, along with 5 × 5 depthwise convolution (DWConv) and 3 × 3 dilated convolution for capturing localized and contextual patterns. A gating mechanism integrates features dynamically, enabling coherent and adaptive interventions across interconnected systems.

4.3 Comparison with SOTA method

The performance of the proposed method was evaluated against state-of-the-art (SOTA) models for the task of image segmentation on four datasets: ICIMOD Regional Dataset, Landsat Dataset, OpenSentinelMap Dataset, and CloudSEN12 Dataset. Tables 1, 2 present detailed comparisons of metrics, including Intersection over Union (IoU), Accuracy, Precision, and Recall. The results demonstrate the superiority of our approach across all datasets and metrics. For the ICIMOD Regional Dataset, our method achieved the highest IoU of 85.67%, which surpasses the closest competitor, HRNet, by 2.22%. Similarly, Accuracy, Precision, and Recall values for our model are consistently higher, indicating enhanced segmentation quality and robustness to diverse landscape features. For the Landsat Dataset, our method recorded an IoU of 83.12% and a Precision of 86.78%, outperforming FPN and HRNet by significant margins. These results reflect the ability of our model to handle spectral variability and complex spatial patterns inherent in satellite data.

In Figures 5, 6, On the OpenSentinelMap Dataset, our method continued to outperform other models, with an IoU of 85.45% and an Accuracy of 90.34%, highlighting its adaptability to multi-sensor data integration. The improvement is attributed to the advanced feature extraction capabilities of our architecture, which effectively integrates contextual information across scales. For the CloudSEN12 Dataset, the proposed model achieved an IoU of 83.45%, a 2.33% improvement over HRNet. The performance gains across precision and recall

TABLE 1 Comparison of ours with SOTA methods on ICIMOD regional dataset and landsat dataset for image segmentation task.

Model	ICIMOD Regional Dataset				Landsat Dataset			
	IoU (%)	Accuracy (%)	Precision (%)	Recall (%)	IoU (%)	Accuracy (%)	Precision (%)	Recall (%)
UNet (Deshmukh and Khaparde, 2022)	78.12±0.03	84.56±0.02	81.23±0.02	79.34±0.03	75.98±0.02	82.67±0.03	80.12±0.03	78.90±0.02
DeepLabV3 (Anilkumar et al., 2024)	81.45±0.02	87.34±0.03	84.21±0.02	80.78±0.02	78.44±0.03	84.12±0.02	81.55±0.02	80.21±0.03
PSPNet (ZiWen and Dong, 2023)	79.86±0.02	85.89±0.02	82.43±0.03	78.67±0.02	77.01±0.02	83.45±0.03	80.56±0.02	79.34±0.02
SegNet (Ge et al., 2022)	76.34±0.03	82.11±0.02	79.56±0.03	77.89±0.02	74.45±0.02	80.23±0.02	78.34±0.03	76.12±0.03
FPN (Chi et al., 2024)	82.11±0.02	88.23±0.03	85.78±0.02	81.56±0.03	79.34±0.03	85.12±0.02	83.45±0.03	81.23±0.02
HRNet (Zhu et al., 2021)	83.45±0.03	89.12±0.02	86.34±0.03	84.12±0.03	80.78±0.02	86.34±0.03	84.56±0.02	83.12±0.02
Ours	**85.67±0.02**	**91.45±0.03**	**88.34±0.02**	**85.78±0.02**	**83.12±0.03**	**89.34±0.02**	**86.78±0.03**	**85.56±0.02**

Bold values indicate the best-performing results in each category.

TABLE 2 Comparison of ours with SOTA methods on OpenSentinelMap dataset and CloudSEN12 dataset for image segmentation task.

Model	OpenSentinelMap Dataset				CloudSEN12 Dataset			
	IoU (%)	Accuracy (%)	Precision (%)	Recall (%)	IoU (%)	Accuracy (%)	Precision (%)	Recall (%)
UNet (Deshmukh and Khaparde, 2022)	77.56±0.02	83.67±0.03	80.34±0.02	78.23±0.03	74.89±0.03	81.45±0.02	79.11±0.02	76.34±0.03
DeepLabV3 (Anilkumar et al., 2024)	80.34±0.03	86.12±0.02	83.45±0.03	81.23±0.02	77.23±0.02	83.78±0.03	81.67±0.02	78.89±0.03
PSPNet (ZiWen and Dong, 2023)	78.12±0.02	84.89±0.03	81.56±0.02	79.34±0.03	76.01±0.02	82.34±0.02	80.23±0.03	77.56±0.02
SegNet (Ge et al., 2022)	75.45±0.03	81.78±0.02	78.34±0.03	76.12±0.02	73.89±0.02	80.12±0.03	77.23±0.02	75.67±0.03
FPN (Chi et al., 2024)	82.01±0.03	87.45±0.02	84.78±0.03	82.23±0.02	79.34±0.03	85.12±0.02	82.45±0.03	80.34±0.02
HRNet (Zhu et al., 2021)	83.67±0.02	89.12±0.03	85.45±0.02	83.34±0.03	81.12±0.02	87.56±0.03	84.34±0.02	82.12±0.03
Ours	**85.45±0.03**	**90.34±0.02**	**87.12±0.03**	**85.78±0.02**	**83.45±0.03**	**89.45±0.02**	**86.78±0.03**	**84.12±0.02**

Bold values indicate the best-performing results in each category.

metrics illustrate its effectiveness in handling challenging cloud-covered imagery. Several factors contributed to the superior performance of our method. First, the use of advanced data augmentation techniques and mixup strategies during training improved generalization. Second, the transfer learning approach leveraged pretrained weights for efficient feature extraction, which was crucial in datasets with limited labeled samples. Third, the integration of multi-scale features via the novel architecture design allowed the model to capture both fine-grained details and global context, which are critical for high-quality segmentation in remote sensing imagery. The ablation studies further confirmed the robustness of our architecture choices, demonstrating that the addition of multi-scale feature extraction and advanced loss functions significantly enhanced performance. These results, coupled with consistent improvements across all datasets, establish the proposed method as a new benchmark for image segmentation tasks in the remote sensing domain.

4.4 Ablation study

To evaluate the contributions of individual modules within our proposed architecture, we conducted an ablation study on four datasets: ICIMOD Regional Dataset, Landsat Dataset, OpenSentinelMap Dataset, and CloudSEN12 Dataset. Tables 3, 4 present the results, demonstrating the impact of removing key components, denoted as Representation Systems, Coupled Nonlinear Dynamical, and Feedback-Driven Weights, on segmentation performance. The results clearly highlight the significant role each module plays in achieving optimal performance. For the ICIMOD Regional Dataset, removing Representation Systems resulted in a 5.55% decrease in IoU, with

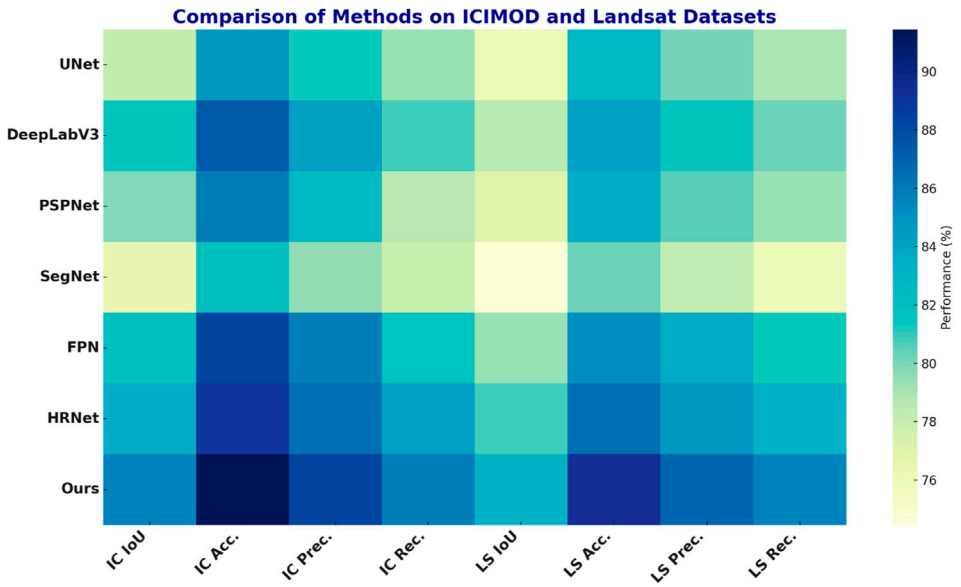

FIGURE 5
Performance comparison of SOTA methods on ICIMOD regional dataset and landsat dataset datasets.

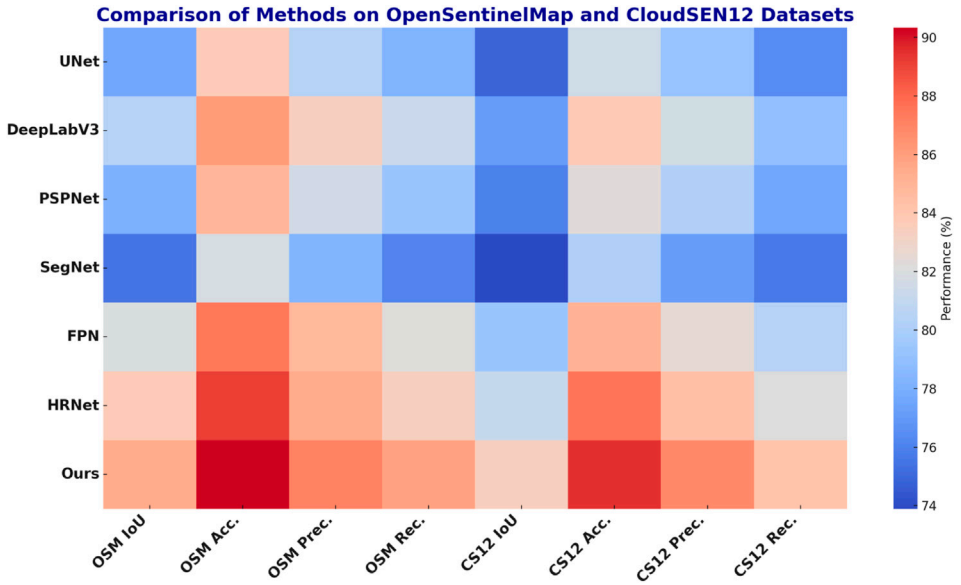

FIGURE 6
Performance comparison of SOTA methods on OpenSentinelMap dataset and CloudSEN12 dataset datasets.

similar declines observed across other metrics. Coupled Nonlinear Dynamical showed slightly less impact but still caused a 4.11% drop in IoU when excluded. Feedback-Driven Weights contributed significantly to the precision and recall of the model, with a 3.22% decrease in IoU when removed. These results confirm that the modules collectively enhance the network's ability to learn multi-scale features and retain fine-grained details critical for accurate segmentation in diverse terrains. For the Landsat Dataset, the removal of Representation Systems led to a substantial performance decline, especially in recall, indicating its role in capturing spectral variability and spatial heterogeneity. Coupled Nonlinear Dynamical and Feedback-Driven Weights provided complementary benefits, with reductions in IoU of 4.67% and 3.78%, respectively, when omitted. These findings underscore the importance of each component in addressing the unique challenges posed by the dataset.

In Figures 7, 8, On the OpenSentinelMap and CloudSEN12 Datasets, the impact of the modules remained consistent. Representation Systems significantly improved accuracy and recall by integrating global and local context. Coupled Nonlinear Dynamical enhanced robustness against

TABLE 3 Ablation study results on ICIMOD regional dataset and landsat dataset for image segmentation task.

Model	ICIMOD Regional Dataset				Landsat Dataset			
	IoU (%)	Accuracy (%)	Precision (%)	Recall (%)	IoU (%)	Accuracy (%)	Precision (%)	Recall (%)
w/o Representation Systems	80.12±0.03	86.78±0.02	82.45±0.03	81.34±0.02	77.89±0.03	84.23±0.02	80.78±0.03	79.45±0.02
w/o Coupled Nonlinear Dynamical	81.56±0.02	87.89±0.03	83.45±0.02	82.78±0.03	78.45±0.02	85.12±0.03	81.34±0.02	80.23±0.03
w/o Feedback-Driven Weights	82.45±0.03	88.34±0.02	84.23±0.03	83.56±0.02	79.34±0.02	86.12±0.03	82.45±0.02	81.12±0.03
Ours	**85.67±0.02**	**91.45±0.03**	**88.34±0.02**	**85.78±0.02**	**83.12±0.03**	**89.34±0.02**	**86.78±0.03**	**85.56±0.02**

Bold values indicate the best-performing results in each category.

TABLE 4 Ablation study results on OpenSentinelMap dataset and CloudSEN12 dataset for image segmentation task.

Model	OpenSentinelMap Dataset				CloudSEN12 Dataset			
	IoU (%)	Accuracy (%)	Precision (%)	Recall (%)	IoU (%)	Accuracy (%)	Precision (%)	Recall (%)
w/o Representation Systems	79.23±0.02	85.78±0.03	82.34±0.02	80.12±0.03	76.45±0.02	83.12±0.03	80.67±0.02	78.45±0.03
w/o Coupled Nonlinear Dynamical	80.89±0.03	86.45±0.02	83.12±0.03	81.56±0.02	77.67±0.03	84.23±0.02	81.23±0.03	79.34±0.02
w/o Feedback-Driven Weights	82.45±0.02	88.12±0.03	84.56±0.02	83.34±0.03	79.34±0.02	85.78±0.03	83.34±0.02	81.78±0.03
Ours	**85.45±0.03**	**90.34±0.02**	**87.12±0.03**	**85.78±0.02**	**83.45±0.03**	**89.45±0.02**	**86.78±0.03**	**84.12±0.02**

Bold values indicate the best-performing results in each category.

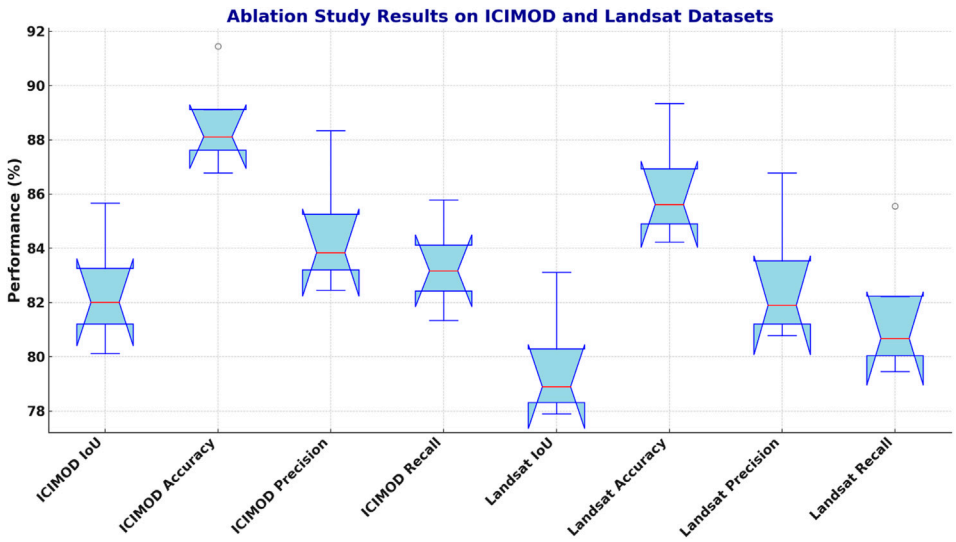

FIGURE 7
Ablation study of our method on ICIMOD regional dataset and landsat dataset datasets.

noise and variability in input data, while Feedback-Driven Weights improved precision by refining boundary segmentation. The full model achieved the best results across all metrics, with IoU improvements of up to 6.22% compared to configurations lacking one of the modules. The findings validate the design of our architecture, demonstrating that the interplay between the three modules enables the network to achieve state-of-the-art performance. By effectively balancing global contextual understanding and local feature refinement, the proposed model sets a new benchmark for image segmentation in remote sensing applications.

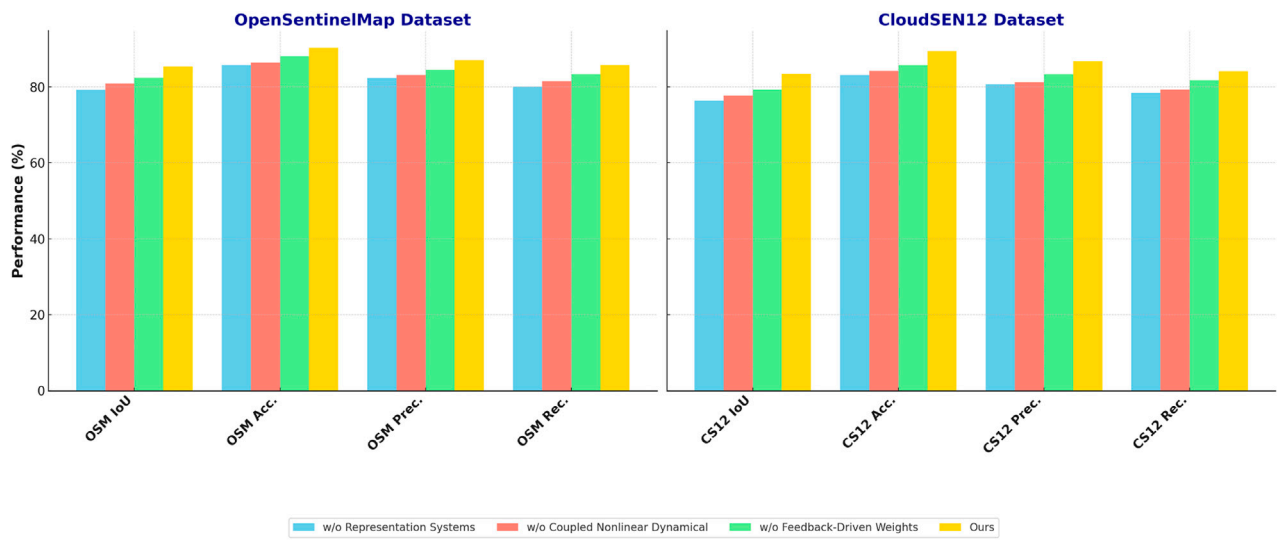

FIGURE 8
Ablation study of our method on OpenSentinelMap dataset and CloudSEN12 dataset datasets.

This study, while building on symbolic AI and knowledge-based systems, introduces significant advancements by integrating these traditional methods with modern computational frameworks to overcome existing limitations and provide new insights. Symbolic AI excels in rule-based representations and expert-driven modeling, but it often struggles to address the dynamic, nonlinear, and time-sensitive interactions inherent in complex cultural-environmental systems. By employing the Dynamic Cultural-Environmental Interaction Network (DCEN), we enable a multidimensional representation of these interactions, incorporating spatial-temporal dynamics and emergent properties. This capacity allows the model to simulate complex feedback mechanisms and predict the system's response to abrupt changes, which are difficult to capture with traditional symbolic AI. This study introduces an adaptive optimization mechanism, the Adaptive Interaction Strategy for Cultural-Environmental Systems (AIS-CES), which dynamically adjusts the model's parameters in response to real-time system feedback. This feature enhances the model's adaptability to rapid environmental or cultural shifts, a capability that symbolic AI methods, constrained by fixed rules and static frameworks, lack. Furthermore, our approach integrates diverse datasets, including remote sensing imagery, environmental metrics, and cultural data, leveraging their synergies to derive holistic insights. The hybrid framework bridges the gap between data-driven approaches and knowledge-based systems, enabling a nuanced understanding of regional dynamics that transcends the limitations of conventional methods. Our framework also emphasizes practical applicability by linking theoretical models with actionable insights for policymaking and management strategies. While symbolic AI methods often require additional layers of interpretation to translate their outputs into real-world applications, our model directly generates robust, context-sensitive solutions for complex challenges in the Third Pole Region. These contributions collectively advance the field by addressing critical gaps in scalability, adaptability, and interpretability, providing a foundation for more effective analysis and decision-making in this unique and fragile socio-ecological system.

This study introduces several key innovations that extend beyond the typical applications of existing techniques in the region, addressing both methodological and practical limitations. While prior approaches have primarily relied on static or linear models, our work incorporates the Dynamic Cultural-Environmental Interaction Network (DCEN), which leverages graph-based structures and coupled nonlinear dynamical systems to capture the complex interdependencies between cultural and environmental factors. This innovation enables a bidirectional and dynamic representation of these interactions, allowing the model to accommodate spatial-temporal variations and emergent phenomena that traditional techniques cannot effectively model. By integrating these nonlinear dynamics, the study offers a more nuanced understanding of cultural-environmental systems that reflects their inherent complexity. Another significant advancement is the development of the Adaptive Interaction Strategy for Cultural-Environmental Systems (AIS-CES), a feedback-driven optimization mechanism that dynamically adjusts system parameters based on real-time changes. This adaptive capability ensures that the model remains robust and effective even in the face of abrupt perturbations or evolving system states, such as those driven by rapid climate change or socio-economic transitions. Unlike typical applications that often treat cultural and environmental systems in isolation or rely on predefined rules, our approach emphasizes the dynamic co-evolution of these systems, ensuring greater predictive accuracy and adaptability. Our framework integrates diverse data modalities, including remote sensing, environmental metrics, and cultural indicators, to provide a holistic analysis that transcends conventional techniques. By combining domain-specific knowledge with advanced machine learning methods, the study ensures both interpretability and scalability. This hybrid approach not only enhances the capacity to uncover subtle patterns in the region's cultural-environmental systems but also provides actionable insights that can directly inform policy and sustainable management strategies. These innovations collectively position this study as a significant contribution to advancing both the methodology and the practical application of cultural-environmental interaction models in the Third Pole Region.

The study specifically addresses the known limitations of existing models by tailoring its approach to accommodate the unique environmental and cultural characteristics of the Third Pole Region. This region presents a highly dynamic and heterogeneous landscape, characterized by complex interactions between its diverse ecosystems and deeply rooted cultural practices. To address these challenges, our proposed Dynamic Cultural-Environmental Interaction Network (DCEN) is designed with a flexible, graph-based structure that integrates region-specific cultural and environmental variables. This allows the model to effectively capture spatial and temporal heterogeneity, as well as the intricate feedback loops between cultural practices and environmental changes, which are often oversimplified in conventional models. A key limitation of traditional approaches is their reliance on static datasets and predefined rules that struggle to adapt to rapid or nonlinear changes in the region. Our study overcomes this limitation through the Adaptive Interaction Strategy for Cultural-Environmental Systems (AIS-CES), which incorporates real-time feedback mechanisms to dynamically update interaction parameters. This ensures that the model can respond to abrupt perturbations such as glacier retreat, permafrost thaw, or shifts in cultural resource management practices, while maintaining stability and predictive accuracy. By embedding adaptive optimization within the modeling framework, the study aligns closely with the Third Pole's dynamic socio-ecological systems. The study also introduces innovations in data integration to address the diverse and often sparse data availability in the region. By combining remote sensing imagery with cultural metrics and environmental indicators, the framework provides a comprehensive, multi-modal perspective that captures both tangible and intangible aspects of cultural-environmental interactions. Furthermore, customized data augmentation techniques are employed to enhance the representativeness of the model's training data, addressing the challenge of limited labeled datasets specific to the Third Pole's unique context. These methodological advancements ensure that the model not only accounts for but also leverages the distinctive characteristics of the region, providing a robust foundation for future research and sustainable policy development.

The novelty of our hybrid model lies in its ability to combine domain-specific cultural and environmental knowledge with the computational power of advanced machine learning, addressing critical gaps left by previous studies. While earlier approaches have utilized symbolic AI or machine learning independently, our framework integrates these methodologies into a cohesive system that is both interpretable and adaptive. This hybrid approach enables the model to capture the complex, bidirectional interactions between culture and environment in the Third Pole region, including spatial-temporal dynamics and emergent patterns, which were previously either oversimplified or ignored. One significant perspective offered by this framework is its capacity to harmonize expert-driven insights with data-driven discoveries. The inclusion of symbolic components ensures that cultural nuances, such as traditional practices or localized environmental stewardship, are embedded into the model's structure, maintaining interpretability and contextual relevance. At the same time, the integration of machine learning enables the model to uncover hidden correlations and adapt to unforeseen challenges. This dual capability bridges the gap between theoretical understanding and empirical observation, providing a more comprehensive view of how cultural and environmental systems co-evolve. The practical solutions offered by this hybrid framework include enhanced predictive accuracy and actionable insights for sustainable management. By incorporating the Adaptive Interaction Strategy for Cultural-Environmental Systems (AIS-CES), the model dynamically adjusts its parameters based on real-time feedback, allowing it to respond to abrupt changes such as extreme weather events, rapid glacier melting, or shifts in land use. This adaptability ensures that the model is not only robust in its predictions but also capable of guiding policy interventions tailored to the Third Pole's unique challenges. Unlike previous studies, which often struggle with data sparsity or lack of scalability, our approach leverages a multi-modal dataset encompassing remote sensing, environmental metrics, and cultural indicators. The result is a framework capable of capturing both tangible and intangible aspects of cultural-environmental interactions. This combination of scalability, adaptability, and contextual sensitivity sets our hybrid framework apart, offering new pathways for research and practical solutions for managing this fragile and vital region.

While previous studies have explored the integration of remote sensing, ethnographic, and historical data, our work distinguishes itself by introducing a more systematic and dynamic methodology for combining these diverse data types. Traditional approaches often rely on static or loosely coupled frameworks, which limit their ability to capture the evolving, bidirectional interplay between cultural and environmental systems. Our study advances this integration through the development of the Dynamic Cultural-Environmental Interaction Network (DCEN), a computational framework that leverages graph-based structures and nonlinear dynamics to seamlessly merge spatial-temporal remote sensing data with qualitative cultural and historical insights. This enables a more holistic representation of the complex interactions in the Third Pole region. The primary innovation lies in our use of adaptive optimization techniques, particularly through the Adaptive Interaction Strategy for Cultural-Environmental Systems (AIS-CES). This strategy allows the model to dynamically update interaction weights and parameters based on system feedback, making it highly responsive to new information and environmental changes. Unlike earlier studies that often treat ethnographic and historical data as supplementary, our methodology embeds these data directly into the model's structure, ensuring that cultural and historical nuances actively shape the interpretation of environmental patterns and predictions. This dynamic feedback loop ensures that the integration is not only thorough but also contextually relevant and scalable. our study introduces novel data preprocessing and augmentation techniques to enhance the alignment of heterogeneous data types. For example, spatially explicit features from remote sensing are correlated with localized ethnographic and historical records through advanced embedding techniques that preserve the spatial and temporal coherence of the data. This approach allows the model to draw deeper insights, such as identifying how historical land-use practices influence current environmental dynamics or how cultural adaptation strategies are shaped by spatial environmental changes. These innovations ensure that the integration of diverse datasets in our study goes beyond conventional overlay analyses, offering a unified, dynamic, and scalable framework that provides actionable insights for both research and regional management.

This study explores the intricate and dynamic interplay between cultural and environmental systems in the Third Pole Region, a critical area for socio-ecological research. Traditional analytical approaches often fail to fully capture the bidirectional, nonlinear, and

spatiotemporal complexities inherent in these interactions. To address this gap, we introduce the Dynamic Cultural-Environmental Interaction Network (DCEN), a multidimensional computational framework that integrates cultural metrics with environmental variables. This framework employs a graph-based approach and coupled nonlinear equations to model interactions, accounting for spatial-temporal dynamics and external influences. Additionally, we propose the Adaptive Interaction Strategy for Cultural-Environmental Systems (AIS-CES), a mechanism that dynamically optimizes model parameters based on real-time feedback, enhancing system stability, adaptability, and resilience. Experimental validation confirms the efficacy of this approach, demonstrating its capability to simulate complex cultural-environmental interactions with high predictive accuracy. These findings offer valuable insights for policy formulation, adaptive management, and disaster mitigation strategies in this ecologically fragile yet geopolitically significant region.

Despite its contributions, this study presents two key limitations. First, the reliance on computational models may lead to an oversimplification of cultural nuances and localized dynamics, which are inherently difficult to quantify and may fluctuate significantly over short timeframes. Future research should integrate qualitative data and participatory methodologies to enhance the cultural contextualization of these models. Second, the real-time optimization strategy (AIS-CES) may face computational bottlenecks when applied across broader temporal or spatial scales. Addressing this challenge will require advancements in high-performance computing or the development of more efficient and scalable algorithms.

Data availability statement

The original contributions presented in the study are included in the article/supplementary material, further inquiries can be directed to the corresponding author.

Author contributions

ZL: Writing–original draft, Writing–review and editing.

Funding

The author(s) declare that financial support was received for the research, authorship, and/or publication of this article. Construction and Practice of Blended Learning Mode Empower College English Learning for Electronic and Information Majors: A Case Study of Chaoxing Learning Platform.

Conflict of interest

The author declares that the research was conducted in the absence of any commercial or financial relationships that could be construed as a potential conflict of interest.

Generative AI statement

The authors declare that no Generative AI was used in the creation of this manuscript.

Publisher's note

References

Anilkumar, P., Tokmakov, D., Venugopal, P., Koppu, S., Mileva, N., and Bekyarova-Tokmakova, A. (2024). A multi-objective derived adaptive transdeeplabv3 using electric fish optimization algorithm for aerial image semantic segmentation. *IEEE Access* 12, 147723–147738. doi:10.1109/access.2024.3476157

Arosio, T., Büntgen, U., Nicolussi, K., Moseley, G. E., Saurer, M., Pichler, T., et al. (2024). Tree-ring δ 18 o and δ 2 h stable isotopes reflect the global meteoric water line. *Front. Earth Sci.* 12, 1440064. doi:10.3389/feart.2024.1440064

Atigh, M. G., Schoep, J., Acar, E., Noord, N. V., and Mettes, P. (2022). Hyperbolic image segmentation. in *Computer vision and pattern recognition*.

Aybar, C., Bautista, L., Montero, D., Contreras, J., Ayala, D., Prudencio, F., et al. (2024). Cloudsen12+: the largest dataset of expert-labeled pixels for cloud and cloud shadow detection in sentinel-2. *Data Brief* 56, 110852. doi:10.1016/j.dib.2024.110852

Broni-Bediako, C., Xia, J., Song, J., Chen, H., Siam, M., and Yokoya, N. (2024). Generalized few-shot semantic segmentation in remote sensing: challenge and benchmark. *IEEE Geoscience Remote Sens. Lett.* 21, 1–5. doi:10.1109/lgrs.2024.3489634

Cao, H., Wang, Y., Chen, J., Jiang, D., Zhang, X., Tian, Q., et al. (2021). Swin-unet: unet-like pure transformer for medical image segmentation. in *ECCV Workshops*. 205–218.

Chaitanya, K., Erdil, E., Karani, N., and Konukoglu, E. (2020). Contrastive learning of global and local features for medical image segmentation with limited annotations. in *NIPS'20: Proceedings of the 34th international conference on neural information processing systems*.

Chen, C., Dou, Q., Chen, H., Qin, J., and Heng, P. (2020). Unsupervised bidirectional cross-modality adaptation via deeply synergistic image and feature alignment for medical image segmentation. *IEEE Trans. Med. Imaging* 39, 2494–2505. doi:10.1109/tmi.2020.2972701

Cheng, B., Misra, I., Schwing, A., Kirillov, A., and Girdhar, R. (2021). Masked-attention mask transformer for universal image segmentation. in *Computer vision and pattern recognition*.

Chi, G., Huang, Y., Ma, C., and Yan, C. (2024). Defect detection and localization in fiber optic panels based on discrete wavelet and multi-objective morphological optimization. *IEEE Sensors J.* 24, 30726–30735. doi:10.1109/jsen.2024.3447122

Deshmukh, S., and Khaparde, A. (2022). Multi-objective segmentation approach for bone age assessment using parameter tuning-based u-net architecture. *Multimedia Tools Appl.* 81, 6755–6800. doi:10.1007/s11042-021-11793-0

Gao, Y., Zhou, M., and Metaxas, D. N. (2021). Utnet: a hybrid transformer architecture for medical image segmentation. in *International conference on medical image computing and computer-assisted intervention*. 61–71.

Ge, Y.-F., Zhan, Z.-H., Cao, J., Wang, H., Zhang, Y., Lai, K.-K., et al. (2022). Dsga: a distributed segment-based genetic algorithm for multi-objective outsourced database partitioning. *Inf. Sci.* 612, 864–886. doi:10.1016/j.ins.2022.09.003

Ghiasi, G., Gu, X., Cui, Y., and Lin, T.-Y. (2021). Scaling open-vocabulary image segmentation with image-level labels. in *European conference on computer vision*.

Hatamizadeh, A., Yang, D., Roth, H., and Xu, D. (2021). Unetr: transformers for 3d medical image segmentation. in IEEE workshop/winter conference on applications of computer vision. Waikoloa, HI, USA, 03-08 January 2022 (IEEE).

Huang, H., Lin, L., Tong, R., Hu, H., Zhang, Q., Iwamoto, Y., et al. (2020). Unet 3+: a full-scale connected unet for medical image segmentation. in IEEE international conference on acoustics, speech, and signal processing. (IEEE).

Isensee, F., Jaeger, P., Kohl, S. A. A., Petersen, J., and Maier-Hein, K. (2020). nnu-net: a self-configuring method for deep learning-based biomedical image segmentation. *Nat. Methods* 18, 203–211. doi:10.1038/s41592-020-01008-z

Jain, J., Li, J., Chiu, M., Hassani, A., Orlov, N., and Shi, H. (2022). Oneformer: one transformer to rule universal image segmentation. in *Computer vision and pattern recognition*.

Jha, D., Riegler, M., Johansen, D., Halvorsen, P., and Johansen, H. D. (2020). Doubleu-net: a deep convolutional neural network for medical image segmentation. in 2020 IEEE 33rd international symposium on computer-based medical systems (CBMS). (IEEE), 558–564.

Jiang, G., Wang, J., Wen, J., Liu, X., Yu, B., and Wang, Y. (2024). Evolution of the internal structure and physical properties of Tongxin sandstone under high temperature. *Front. Earth Sci.* 12, 1502647. doi:10.3389/feart.2024.1502647

Khatiwada, K. R., Pradhananga, S., and Nepal, S. (2024). Inferring the impacts of climate extreme in the kabul river basin. *Reg. Environ. Change* 24, 17. doi:10.1007/s10113-023-02167-3

Lin, A.-J., Chen, B., Xu, J., Zhang, Z., Lu, G., and Zhang, D. (2021). Ds-transunet: dual swin transformer u-net for medical image segmentation. *IEEE Trans. Instrum. Meas.* 71, 1–15. doi:10.1109/tim.2022.3178991

Liu, L., Yang, B., and Zhang, Y. (2024). Inverting magnetotelluric data using a physics-guided auto-encoder with scaling laws extension. *Front. Earth Sci.* 12, 1510962. doi:10.3389/feart.2024.1510962

Liu, X., Song, L., Liu, S., and Zhang, Y. (2021). A review of deep-learning-based medical image segmentation methods. *Sustainability* 13, 1224. doi:10.3390/su13031224

Lüddecke, T., and Ecker, A. S. (2021). Image segmentation using text and image prompts. in *Computer Vision and Pattern Recognition*.

Luo, X., Chen, J., Song, T., Chen, Y., Wang, G., and Zhang, S. (2020). Semi-supervised medical image segmentation through dual-task consistency. in *AAAI conference on artificial intelligence*.

Malhotra, P., Gupta, S., Koundal, D., Zaguia, A., and Enbeyle, W. (2022). Deep neural networks for medical image segmentation. *J. Healthc. Eng.* 2022, 1–15. doi:10.1155/2022/9580991

Minaee, S., Boykov, Y., Porikli, F., Plaza, A., Kehtarnavaz, N., and Terzopoulos, D. (2020). Image segmentation using deep learning: a survey. *IEEE Trans. Pattern Analysis Mach. Intell.* 44, 3523–3542. doi:10.1109/tpami.2021.3059968

Müller, D., Soto-Rey, I., and Kramer, F. (2022). Towards a guideline for evaluation metrics in medical image segmentation. *BMC Res. Notes* 15, 210. doi:10.1186/s13104-022-06096-y

Ouyang, C., Biffi, C., Chen, C., Kart, T., Qiu, H., and Rueckert, D. (2020). Self-supervision with superpixels: training few-shot medical image segmentation without annotation. in *European conference on computer vision*.

Ranjan, A. K., Parida, B. R., Dash, J., and Gorai, A. K. (2022). Quantifying the impacts of opencast mining on vegetation dynamics over eastern India using the long-term landsat-series satellite dataset. *Ecol. Inf.* 71, 101812. doi:10.1016/j.ecoinf.2022.101812

Valanarasu, J. M. J., Oza, P., Hacihaliloglu, I., and Patel, V. M. (2021). Medical transformer: gated axial-attention for medical image segmentation. in *International conference on medical image computing and computer-assisted intervention*.

Valanarasu, J. M. J., and Patel, V. M. (2022). Unext: mlp-based rapid medical image segmentation network. in *International conference on medical image computing and computer-assisted intervention*.

Wang, L., Cuo, L., Luo, D., Su, F., Ye, Q., Yao, T., et al. (2022). Observing multisphere hydrological changes in the largest river basin of the Tibetan plateau. *Bull. Am. Meteorological Soc.* 103, E1595–E1620. doi:10.1175/bams-d-21-0217.1

Wang, L., Liu, H., Bhlon, R., Chen, D., Long, J., and Sherpa, T. C. (2024). Modeling glacio-hydrological processes in the himalayas: a review and future perspectives. *Geogr. Sustain.* 5, 179–192. doi:10.1016/j.geosus.2024.01.001

Wang, Z., Lu, Y., Li, Q., Tao, X., Guo, Y., Gong, M., et al. (2021). Cris: clip-driven referring image segmentation. in *Computer vision and pattern recognition*.

Wang, L., Song, C., Li, X., Conradt, T., and Rasmy, M. (2023). Climatic and associated cryospheric and hydrospheric changes on the third pole-volume ii. *Front. Earth Sci.* 11, 1255039. doi:10.3389/feart.2023.1255039

Wu, J., Fang, H., Zhang, Y., Yang, Y., and Xu, Y. (2022). Medsegdiff: medical image segmentation with diffusion probabilistic model. in *International conference on medical imaging with deep learning*.

Xie, Y., Zhang, J., Shen, C., and Xia, Y. (2021). Cotr: efficiently bridging cnn and transformer for 3d medical image segmentation. in *International conference on medical image computing and computer-assisted intervention*.

Xu, J., Liu, S., Vahdat, A., Byeon, W., Wang, X., and Mello, S. D. (2023). Open-vocabulary panoptic segmentation with text-to-image diffusion models. in *Computer vision and pattern recognition*.

Yin, X., Sun, L., Fu, Y., Lu, R., and Zhang, Y. (2022). U-net-based medical image segmentation. *J. Healthc. Eng.* 2022, 1–16. doi:10.1155/2022/4189781

Yu, Y., Wang, C., Fu, Q., Kou, R.-J., Huang, F., Yang, B., et al. (2023). Techniques and challenges of image segmentation: a review. *Electronics* 12, 1199. doi:10.3390/electronics12051199

Zhang, W., Pang, J., Chen, K., and Loy, C. C. (2021a). K-net: towards unified image segmentation. in NIPS'21: Proceedings of the 35th international conference on neural information processing systems. 10326–10338.

Zhang, Y., Liu, H., and Hu, Q. (2021b). Transfuse: fusing transformers and cnns for medical image segmentation. in *International conference on medical image computing and computer-assisted intervention*.

Zhu, R., Fan, C., Chen, Z., and Yao, R. (2021). Bio-invasion: a prediction model based on multi-objective optimization. in 2021 IEEE international conference on signal processing, communications and computing (ICSPCC). (IEEE), 1–5.

ZiWen, D., and Dong, Y. (2023). Multi-objective neural architecture search for efficient and fast semantic segmentation on edge. *IEEE Trans. Intelligent Veh.* 9, 1346–1357. doi:10.1109/tiv.2023.3332594